TECHNISCHE
UNIVERSITÄT
WIEN

VIENNA
UNIVERSITY OF
TECHNOLOGY

DIPLOMARBEIT

Beam Phase and Intensity Monitoring for the Compact Muon Solenoid Experiment

Ausgeführt am

ATOMINSTITUT DER ÖSTERREICHISCHEN UNIVERSITÄTEN

unter der Anleitung von

UNIV.DOZ. UNIV.PROF. DR. DIPL.-ING. CHRISTIAN FABJAN

durch

THOMAS AUMEYR
Kirchbach 15
4720 Neumarkt/H.
Austria
e0226202@student.tuwien.ac.at

2. April 2008

Declaration

I declare that this thesis is my own work and has not been submitted in any form for another degree or diploma at any university or other institution of tertiary education. Information derived from the published or unpublished work of others has been acknowledged in the text and a list of references is given.

Vienna, 2nd April 2008

Thomas Aumeyr

Zusammenfassung

Das Compact Muon Solenoid (CMS) Experiment ist ein großer Teilchendetektor am Large Hadron Collider (LHC), einem Proton-Proton-Ringbeschleuniger am CERN. Im Inneren von CMS werden Protonenpakete alle 25 ns ihre Bahnen kreuzen. Die Protonenpakete werden eine Energie von 7 TeV besitzen, was in einer Gesamtkollisionsenergie von 14 TeV resultiert. Verschiedene Subdetektoren, wie z.B. Tracker, Spektrometer and Kalorimeter, werden diese Kollisionen untersuchen. Um eine korrekte Zeitsteuerung der Datenaufnahme in den Subdetektoren zu garantieren, muss eine konstante Phase zwischen einem Taktsignal und den Ankunftszeiten der Protonenpakete im Detektor eingehalten werden.

Der Schwerpunkt dieser Arbeit liegt in der Entwicklung, der Umsetzung und dem Testen eines Systems genannt Beam Pick-Up Timing Experiment (BPTX). Das System besteht aus zwei elektrostatischen Pick-Up-Stationen, die ungefähr 175 m vom Interaktionspunkt entfernt auf beiden Seiten des Detektors installiert wurden. Die Pick-Up-Detektoren setzen sich aus vier Kreiselektroden zusammen und wurden entlang des LHCs gebaut, um die Teilchenstrahlen zu überwachen. Jedes Protonenpaket, das eine dieser beiden Stationen passiert, erzeugt ein Signal, welches sowohl für die Überwachung der Zeitsteuerung und der Struktur der einfallenden Strahlen als auch der Kenndaten der einzelnen Pakete verwendet werden kann.

Das Ausleseverfahren für das BPTX-System basiert auf der Verwendung eines kommerziellen 4-Kanal-Oszillskops, das alle 1-2 Sekunden einen ganzen LHC-Orbit mit einer Zeitauflösung von 200 ps aufzeichnen wird. Nachdem die Verarbeitungssoftware die interessanten Parameter jedes einzelnen Pakets (Länge, Intensität und Ankunftszeit) bestimmt hat, wird die Phase in Verhältnis zum Takt des Experiments berechnet. Diese Information kann dann dazu verwendet werden, die Phasenverschiebung des Takts abzustimmen.

Da die Signale von den BPTX-Detektoren auch Informationen über das Füllschema der zwei Teilchenstrahlen enthalten, bietet das System darüberhinaus eine Möglichkeit, deren Struktur zu überwachen. Daher können sogenannte Geisterpakete maßgeblicher Größe erkannt werden.

Abstract

The Compact Muon Solenoid (CMS) experiment is a large general-purpose particle physics detector on the proton-proton Large Hadron Collider (LHC) at CERN. Inside CMS bunches of protons will cross paths every 25 ns. The proton bunches will each have an energy of 7 TeV, resulting a total collision energy of 14 TeV. Various subdetectors such as trackers, spectrometers and calorimeters will study these interactions. To ensure correct timing of the data taking in the subdetectors, the stable phase between a clock signal and the bunch crossing must be maintained.

The focus of this thesis is the design, implementation and testing of a system called the Beam Pick-up Timing Experiment (BPTX). It is a system of two electrostatic pick-up stations installed on each side of the detector, about 175 m away from Point 5. Consisting of four button electrodes, the pick-up detectors are installed along the LHC to monitor the incoming beams. Each proton bunch passing by one of these stations causes a signal which can be used for monitoring the timing and the structure of the incoming beams as well as the characteristics of individual bunches.

The read-out developed for the BPTX system is based on the use of a commercial 4-channel oscilloscope, which will capture a full LHC orbit every 1-2 seconds with a time resolution of 200 ps. After the processing software determines the interesting parameters for each individual bunch (i.e. length, intensity, amplitude and arrival time), the phase with respect to the experimental clock is calculated. This information can then be used to adjust the phase shift of the clock.

In addition, since the signals from the BPTX detectors also contain information about the filling scheme of the two particle beams, the system can provide a possibility of monitoring their structure. Thus, so-called ghost bunches of significant size can be identified.

Acknowledgements

With all my heart I would like to thank my supervisors at CERN, Alick Macpherson and Richard Hall-Wilton, for giving me all the support and freedom I needed and also taking the time for explanations and discussing results, as well as paying for coffee. I have greatly enjoyed contributing to the BRM group and am deeply grateful for their help. Vladimir Ryjov and Alan Bell always had the time to give feedback or simply a ride to the SPS. Furthermore, I have learned a lot from the cooperation with Thilo Pauly and Christian Ohm, both working on the ATLAS BPTX system, and their contributions.

I would also like to express my gratitude to Christian Fabjan, my examining tutor at Vienna University of Technology, for his constructive criticism and help on bringing this thesis together.

In the end, I would like to thank my flatmate in Geneva, Carlos Ghabrous-Larrea, and my fellow Chez Heine inmates in Vienna for putting up with me during the time it took me writing this report as well as distracting me from doing so.

Vienna, 2nd April 2008

Thomas Aumeyr

Contents

List of Figures

List of Tables

Chapter 1

Introduction

1.1 CERN

The *European Organization for Nuclear Research*, commonly known as CERN, is the world's largest particle physics laboratory and is located just outside Geneva on the border between France and Switzerland. It was founded on 29 September 1954. From the original 12 signatory states of the CERN convention, membership has grown to the present 20 member states. Since its formation, CERN has been providing high-energy physicists with particle accelerators and other infrastructure needed to test theories about the structure of matter and the various forces holding it together.

Many elementary particles do not exist under normal circumstances. High-energy particle accelerators are necessary to investigate the smallest parts of matter. The accelerators at CERN form a sequence where each component gradually boosts the speed of a beam of particles, before injecting it into the next one in the sequence. At present, the final component in this sequence, the *Large Hadron Collider* (LHC), is being built in an 27 km long underground circular tunnel. As protons travel around the LHC, they will be accelerated from a kinetic energy of 450 GeV to 7 TeV. This corresponds to a particle speed between 99.99978278% and 99.999999102% of the speed of light in vacuum.

Superconducting magnets are lined along the accelerator bending the path of the particles to keep them in orbit. Two particle beams, circulating in opposite directions, can travel along the accelerator at the same time by simply using different parts of the magnetic field which these magnets create. At four interaction points along the LHC, the particle beams are steered to 14 TeV head-on collisions. In these collisions the energy density may be so high that supposedly conditions similar to the situation right after the Big Bang are recreated. From this energy, more exotic elementary particles, some with a very short lifetime, will then be formed. Around each interaction point, experiments are built in order to look for these subatomic particles and physical phenomena and thus trying study some of the main open issues, such as the origin of particle mass, dark matter or the matter-antimatter-imbalance.

Enormous amounts of data, about 15 PB (1 Petabyte = 10^{15} bytes) per year, are generated by the experiments. The analysis requires high computing power
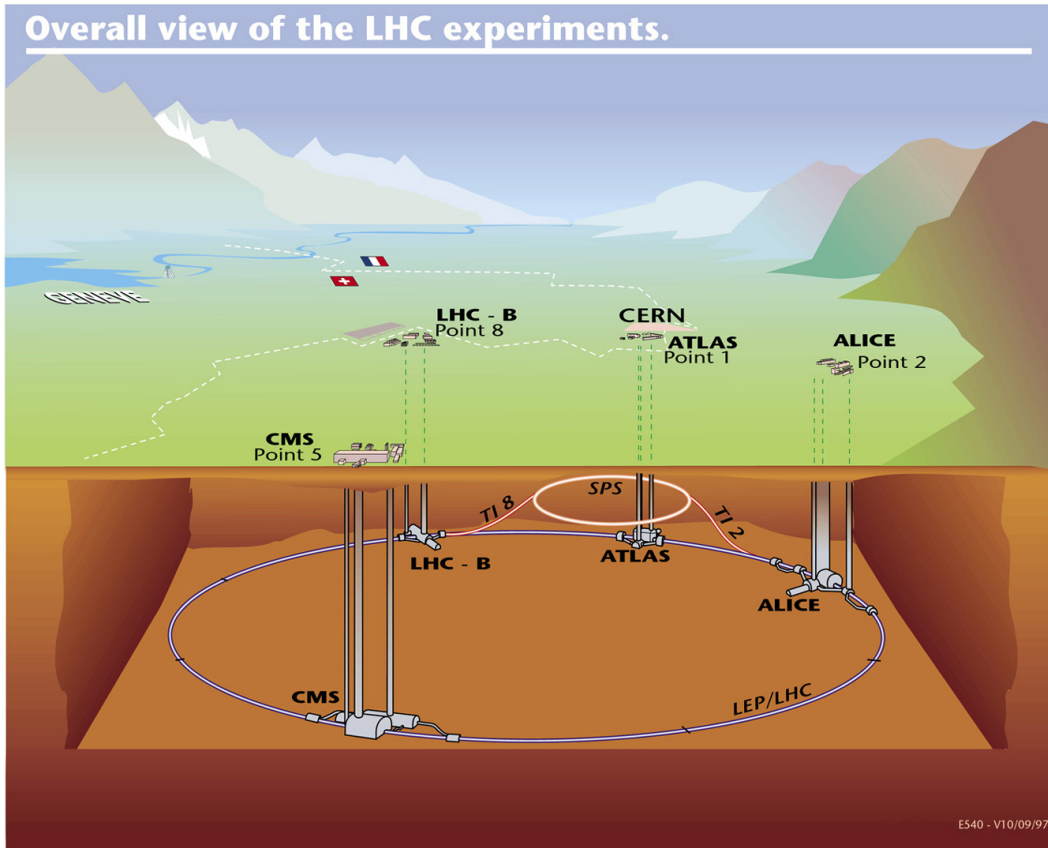
Figure 1.1: ATLAS, ALICE, CMS and LHCb - the four major experiments around the LHC.

and storage capabilities. Therefore, CERN has always used cutting-edge computing and networking technologies to support this advanced experimental research. New "GRID" computing technology will distribute the work load to computer centres all over the world to analyse the data from the LHC experiments. The most notable recent breakthrough in computer science was the birth of the World Wide Web developed by Tim Berners-Lee when creating a hypertext system for exchanging research results within the scientific community.

1.1.1   The CMS experiment at CERN

An underground cavern at *Interaction point 5* (IP 5) near Cessy in France houses CMS, the *Compact Muon Solenoid* experiment, at the LHC. The key aspects of the experiment are the relatively small size, the very strong solenoid magnet and its special ability to detect muon traces. The large solenoid magnet will allow for determining the particle momenta via measuring the bending radius of the particle trajectory. This will allow to identify which particles were generated at the collision of the two high energy proton beams and which kinetic energy they had.

The Standard Model of particle physics is the most widely accepted theoretical
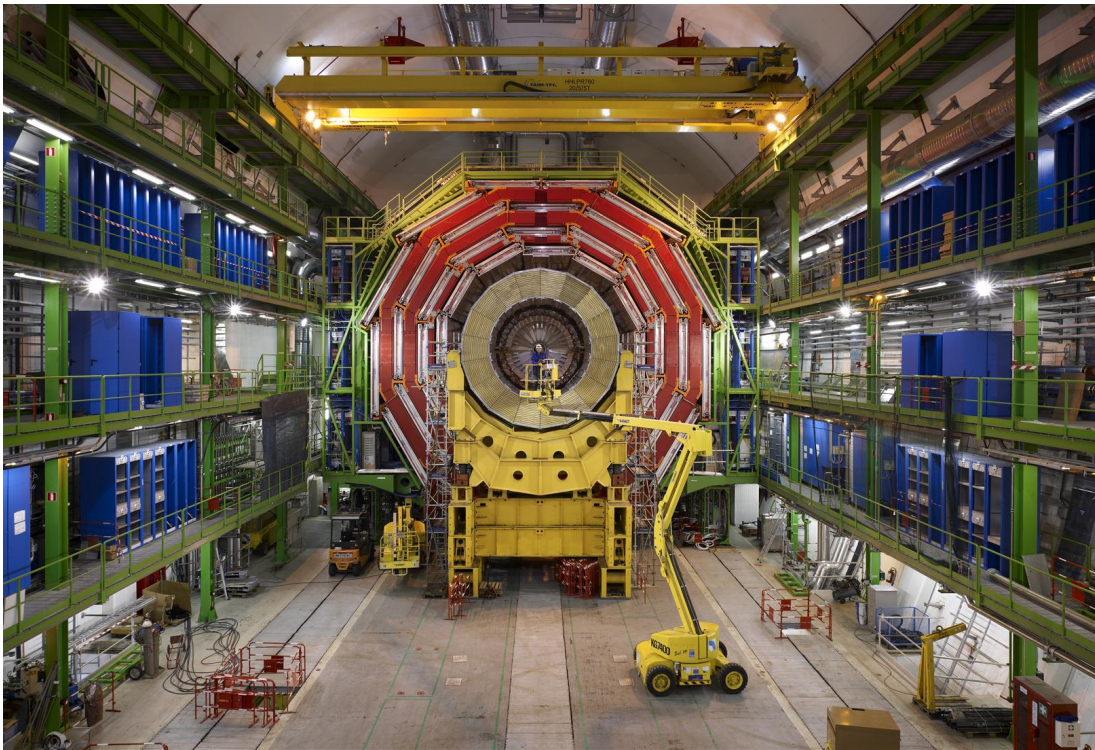
Figure 1.2: View of the CMS cavern with the first half part of the experiment lowered.

model. It describes three of the four known fundamental interactions between the elementary particles that make up all matter. The Higgs particle is a hypothetical massive elementary particle predicted by the Standard Model, and the only fundamental particle predicted by that model which has not been observed as yet. It plays a key role in explaining the origins of the mass of other elementary particles. Finding this Higgs particle is one of the main targets of the CMS detector, besides looking for evidence for supersymmetry and studying collisions of heavy Ions.

1.2 Description of the problem – Monitoring the LHC beam

Instead of being spatially distributed in a uniform way, the particles in the accelerator are grouped together in so-called *bunches*. The bunches consist of over a billion protons. This intensity is different for the various operating modes, but at normal intensity a bunch will contain $1.15 \cdot 10^{11}$ protons (see Section 4.4). The bunches are filled into the LHC according to a *bunch pattern* and they will cross paths at a rate of about 40 MHz. Because of this interaction periodicity, the data taking in the subdetectors is synchronised to a clock signal. Since the way the data is taken is sensitive to the phase between this clock and the bunch crossings, the phase of the clock must be tuned precisely to optimise the signal sampling. Information about the location of the bunches inside the beam pipe allows to calibrate the timing of

the subdetectors.

This clock signal is transmitted to IP 5 through kilometres of optical fibre, which is unfortunately not compensated for temperature. Therefore, the phase of the clock reaching the experiment will shift following changes of weather conditions. If this is not monitored, the subdetectors would sample the signals at incorrect times and therefore possibly miss important data. Monitoring the clock and at the same time the actual bunches coming towards CMS, this time difference can be checked and corrected for.

There is a risk that a fraction of a bunch gets separated from the rest when moving through the accelerator sequence and getting injected into the LHC ring. This fraction then forms a so-called *satellite* or *ghost bunch*. It could cause unwanted off-centre collisions that would disturb measurements of collisions in the centre of CMS. Checking the actual beam structure helps detecting these errors.

In this thesis the design, implementation and testing of a system is presented which is able to monitor the phase of the clock signal and the particle bunch structure of the beams and to measure the amplitude, length and intensity of each incoming particle bunch.

1.3 Thesis outline and limitations

The CMS experiment is built by a collaboration formed by approximately 2600 physicists and engineers from 180 scientific institutes. In order to understand the size and complexity of this collaboration, the reader will be provided with a lot of background information to introduce him/her to the context of the beam monitoring system. Therefore, Chapter 2 begins with generally explaining some of the concepts of the physics used in modern particle accelerators. Then, the LHC is dealt with in particular, also discussing its beam production chain defining the structure of the beam. A more in-depth description of the CMS experiment gives details about the trigger system used to reduce the recorded data and the possible timing troubles. It also gives an insight into how the clock signal is distributed and how it can be tuned to meet the demands of subdetectors. A solution to the problem described in Section 1.2 is presented by explaining the beam position monitor pick-ups and their use for beam monitoring purposes.

Chapter 3 specifies the goal of the beam monitoring system and its requirements, followed by a description of the idea and technology chosen for the design of the monitoring system.

The reader is presented with the theoretical calculations of the signals coming from the detectors in Chapter 4. First, the particle bunch itself is modelled. The detector design is then portrayed and the beam pick-up is described mathematically. Finally, an expression for the signal from the pick-up is derived for a given bunch length and intensity. The various particle beam scenarios with different beam energies and bunch intensities are described and the effects of the transmission line and the data acquisition on the signal are shown.

In Chapter 5, the analysing software designed for the beam monitoring system and also the used data structures are described.

The tests and most important results for the monitoring system and its components are shown in Chapter 6. The stability of the data acquisition is tested by capturing and processing a laboratory-generated bunch signal. Furthermore, the measurements from the *Super Proton Synchrotron* (SPS), one of the components in the acceleration sequence, are presented.

The conclusions drawn from these results are summarised in Chapter 7.

The topic of this thesis is the *Beam Pick-up Timing Experiment* (BPTX) at CMS. It will focus on the design and implementation of the data analysis software, identification of hardware requirements and system tests. Information about the integration of the beam monitoring system into other CMS software frameworks is not a part of this document. Debugging and simulation tools will not be discussed either. Furthermore, the LHC has not yet started operation when this report was created and thus no real-life results for the system in its full context can be presented. However, all parts on the system have been thoroughly simulated and tested in the laboratory.

Chapter 2

Theoretical foundations, the LHC and CMS

2.1 Basic principles of accelerators

A general knowledge about the acceleration of particle beams is needed to understand some of their properties. An insight into the basic principles used in accelerators to boost the kinetic energy of beams is given in this section. More details about how accelerators work can be found in [1].

2.1.1 Radio frequency cavities

In cathode ray tubes (CRT), electrons are accelerated by a potential difference. The energy gained in such a way is the product of particle charge and the accelerating voltage. A particle with elementary charge, e, accelerated through an electrostatic potential difference of 1 V increases its energy by 1 eV (1 Electronvolt $= 1.60217646 \cdot 10^{-19}$ J). Accelerators using a single static potential difference are called *electrostatic accelerators*.

In radio frequency linear accelerators, charged particles pass several acceleration sections. This principle of accelerating potential gaps is illustrated in Figure 2.1.
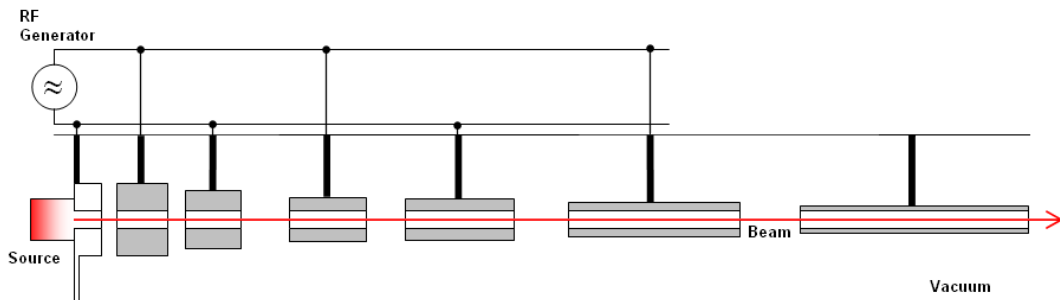
Figure 2.1: Sketch of a drift tube accelerator.

In a drift tube accelerator, developed by Rolf Wideröe, the particles travel through metal tubes, between which a time-varying electrical field is applied. The

field between these cylindrical electrodes is caused by a sinusoidal *radio frequency* (RF) voltage. Inside the tubes the potential is constant and the particles feel no force. The acceleration only happens in the gaps between the tubes. The phase is chosen in a way that the particles always feel an accelerating voltage. To accelerate the particles always at the right moment, the drift time through a tube $\Delta t = L/v$ must be equal to half the frequency period $T/2 = 1/(2f)$. Since the particles gain speed v, the length L of the tubes must increase to have equal drift times L/v and thus be able to keep the radio frequency f constant.

By injecting the particles in a continuous stream, only those arriving at the gap when the field is positive will be accelerated. Additionally, the particles travelling across the gap will increase their energy according to the field magnitude by different amounts. The gaps will then be reached by the particles at different times because of their different velocities. Therefore, the beam energy will be inhomogeneous. If bunches of particles are injected timed to cross the gap during the positive slope of the sinusoidal field, the beam will focus itself along the beam axis. Particles travelling faster than the rest of the bunch will feel a lower field magnitude and will be less accelerated. Particles staying behind will get a higher acceleration and can therefore catch up. Particles going back and forth in a bunch like this follow the so-called *synchrotron oscillation*. This principle is shown in Figure 2.2.
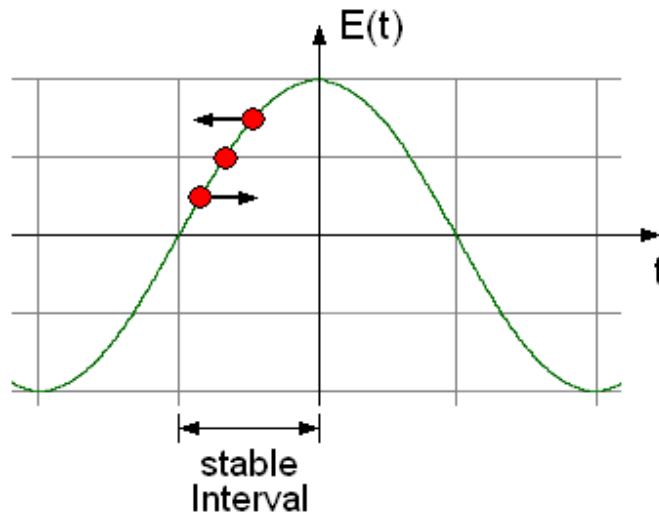
Figure 2.2: Principle of accelerating particles in a drift tube.

In this way, the bunches are located around the accelerator in *buckets* defined by the RF system. Injecting the particles in bunches guarantees a homogeneous beam energy and provides for a beam structure.

Since the particle speed in high energy accelerators approaches the speed of light, relativistic effects can not be neglected anymore. A higher energy will not cause a correspondingly higher speed, but the particles with higher energy will travel in a larger orbit because they will be bent less by the magnets. This effect called *dispersion* causes higher-energetic particles to fall behind. If this happens, the afore-mentioned self-focusing of the beam will only work if the bunch is accelerated by

the negative slope of the sinusoidal field. The dispersion and synchrotron oscillation effects will be equal at a certain beam energy. To ensure a stable phase, it has to be provided for a *transition* where the RF phase quickly switches.

2.1.2 Synchrotrons

RF voltages with higher amplitudes or more drift tubes must be applied to gain more and more energy in the above-mentioned linear accelerator. Building the accelerator in a ring, the gaps could be used over and over again to accelerate the beam. Since particles carry a charge q, their paths can be bent into a circle by magnetic fields.

$$\mathbf{F} = q\mathbf{v} \times \mathbf{B} \tag{2.1}$$

For a long drift tube bent into a circle with only one accelerating gap, every time a bunch travels across the gap, the next turn is going to take less time because of the increasing energy. This will cause the bunch to spread out leading to an eventual deceleration of particles, for the phase of the field will be different for each turn. By increasing the RF frequency precisely according to the beam speed, the phase is kept the same each time the gap is passed. Circulating the beam increases the energy, but this process is limited by the magnetic fields which are responsible to keep the beam on its circular path. Accelerators using this principle are called *synchrotron*. Since such an accelerator is able to store its accelerated beam in circulation for a long period of time, this type is also called a *storage ring*.

In modern accelerators, *resonant cavities* replace the accelerating gaps, but the principle remains the same.

2.2   LHC

The LHC is a synchrotron accelerator able to accelerate two particle beams. Different parts of the field of the bending magnets make it possible that one beam in each direction can be bent around the underground tunnel. It is driven by an RF frequency of about 400 MHz. As the beam speed after being injected from the SPS into the LHC is already close to the speed of light (as mentioned earlier), the RF frequency will increase only slightly as the beam energies are increased to the maximum values. In another accelerator, the Proton Synchrotron (PS), the transition energy is reached where the phase jump is needed to ensure phase stability. Out of the 400 MHz RF buckets only every tenth bucket will be used. Therefore, the two beams are colliding with a bunch crossing frequency of about 40 MHz.

The LHC will primarily be used for accelerating proton beams and three major experiments (ATLAS, CMS and LHCb) are built to study proton-proton collisions. The fourth one, ALICE, is design to study the collisions of heavier atomic nuclei. Thus, the LHC can also be used for accelerating Pb^{82+} ions. This thesis only considers CMS related issues, so that from here on the term "beam" refers to a proton beam.

2.2.1 Beam production chain

As mentioned in Section 1.1, prior to being injected into the LHC, the particles are prepared through a series of systems that successively increase the particle energy levels. The most important parts of the proton and ion beam production are shown in Figure 2.3. Moreover, several filling schemes of the LHC were designed for different operation modes (see [2] for more details).
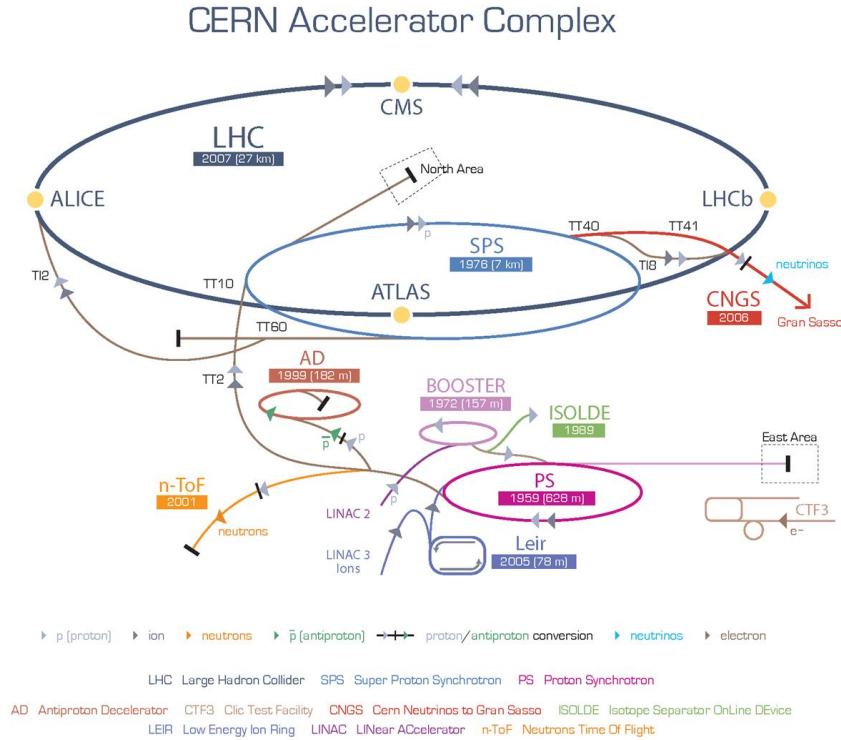
Figure 2.3: The CERN accelerator complex creating the beam production chain.

Proton beam

The first system in the beam production chain is the linear accelerator *Linac2*, generating 50 MeV protons, which feeds the *Proton Synchrotron Booster* (PSB), the first circular accelerator. Protons are then injected into the *Proton Synchrotron* (PS), which will increase the energy from 1.4 GeV to 26 GeV. Finally the *Super Proton Synchrotron* (SPS) is used to increase the energy of the bunched protons up to 450 GeV. This is the injection energy of the LHC, which is able to accelerate the particle bunches up to 7 TeV per beam, thus being the world's highest energy particle accelerator. An in-depth description of the CERN accelerators and their specifications can be found in [3].

Each accelerator in the production sequence is bigger than the previous one. Therefore, the synchrotrons can be filled up with several fillings of the preceding one. To give an example, the production of the "25 ns Scheme" is explained. For

this scheme the PS is filled with 72 bunches. The SPS fill is now built up with a
pattern of two, three or four PS fills per SPS fill. Finally, the LHC is filled with
twelve of these differently long SPS fills. A schematic of the bunch disposition for
this LHC filling scheme is shown in Figure 2.4.
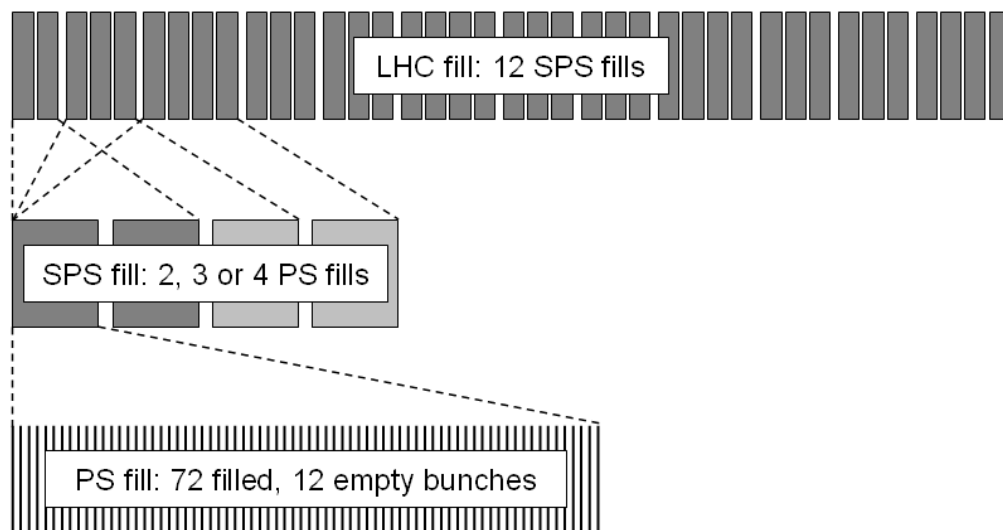
Figure 2.4: Schematic of the bunch disposition around the LHC ring for the "25 ns
Scheme".

This building scheme for the beams is called *bunch pattern*, which defines the
collision structure in the experiments. Since the LHC will have 3564 possible po-
sitions for particle bunches, there are 3564 possible *bunch crossings*. For the "25
ns Scheme" only 2808 bunch locations will actually be filled. The structure of this
beam can be written in terms of PS fills as 234 334 334 334 or in terms of empty (e)
and filled (b) bunch locations as

$$3564 = 2 \times (72b + 8e) + 30e + 3 \times (72b + 8e) + 30e + 4 \times (72b + 8e) + 31e+$$
$$+ 3 \times \{2 \times [3 \times (72b + 8e) + 30e] + 4 \times (72b + 8e) + 31e\} + 80e =$$
$$= 2808b + 756e$$

Errors during the LHC filling may result in bunches being in the wrong RF
buckets. These could cause collisions occurring in off-centre positions in the detectors
and might give rise to problems for the experiments.

When the intensity and quality of the stored beams become insufficient, the beam
is dumped and the LHC pipes are refilled. Dumping the beam is carried out by so-
called *kicker magnets* which bend the beam out of the synchrotron. In order to ramp
up the currents driving the magnets, these kickers need at least a 3 μs time frame.
That is why all filling schemes must have a long gap to give the kickers enough time
to reach full field strength. The LHC filling time per ring is 4.3 minutes.

Ion beam

The production sequence for the Pb^{82+} ion beams is different from the proton beam. The ions will be first accelerated by the linear accelerator *Linac3*, and the *Low Energy Ion Ring* (LEIR) will be used as an ion storage and cooler unit to shorten the long pulses increasing the sharpness of the ion bunches. The ions are then further accelerated by the PS and the SPS. Further details (e.g. beam energies) can be found in [4].

2.3   CMS

Being 21.5 m long and 15 m high, the CMS experiment is only a quarter of the size of its counterpart experiment ATLAS, but with a massive 12500 tons it has about twice the weight. It is built to be a general purpose detector, designed to observe all possible decay products of the 14 TeV proton-proton collisions. Figure 2.5 shows the CMS setup and its different subdetectors.
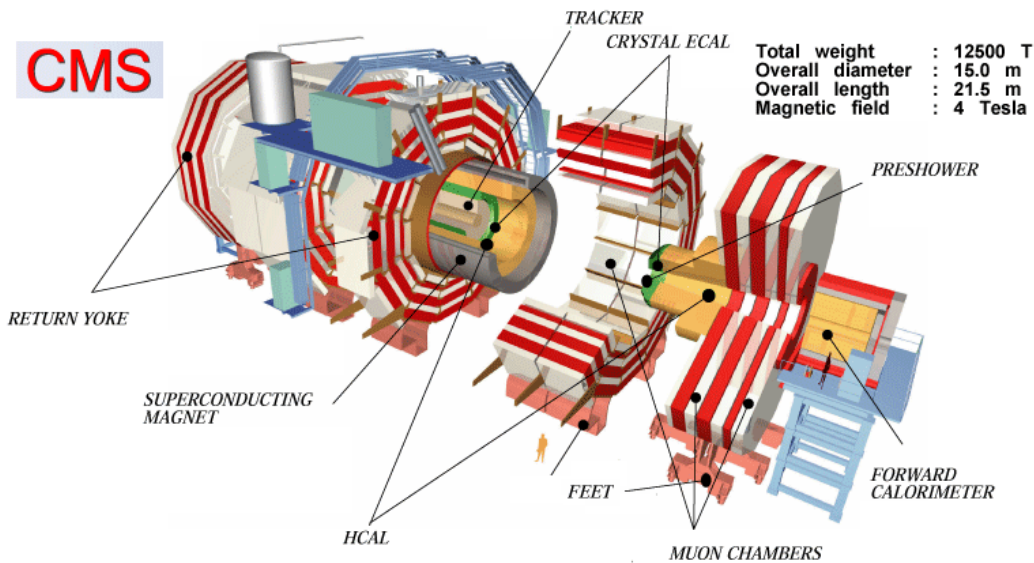
Figure 2.5: An overview of the CMS experiment. In the middle, under the so-called barrel a person provides the scale (HCAL = hadron calorimeter, ECAL = electromagnetic calorimeter).

The Higgs boson, a hypothetical massive elementary particle, is the only particle of the Standard Model of particle physics yet to be found. The reason for this is its supposedly high mass, which could not be produced with existing accelerators. The experimental lower limit for its mass was given by the LEP with 114.1 GeV.

In particle physics, supersymmetry is a symmetry that links elementary particles of one spin to another particle that differs by half a unit of spin. These are known as superpartners. There is no evidence of supersymmetric particles yet, but finding them would provide new hints about how to unify the weak, strong and electromagnetic forces.

The CMS detector will look for these hypothetical particles and find them, if they exist. Furthermore, it will be able to study aspects of heavy ion collisions, which will reproduce conditions of the very early Universe, less than one second after the Big Bang. For more details, the reader is referred to [5].

2.3.1 Trigger system

A vast majority of the collisions in the LHC will result in well-understood physical processes. The trigger represents the start of the physics event selection. For the nominal LHC mode with $1.15 \cdot 10^{11}$ protons per bunch (ppb), an average of 17 proton-proton collisions will occur at the beam crossing frequency of 25 ns. Therefore, the input rate has an order of about 10^9 interactions every second. Since the maximum rate that can be achieved by the online processing is only 100 Hz, the event rate needs to be reduced by at least a factor of 10^7.

For CMS, reducing the event rate is done in two steps. At the first level, all data with identified muons, electrons, photons, jets and missing transverse energy is stored. A decision to keep a data set for an event for further analysis has to be made every 25 ns. After this Level-1 (L1) system, less than 100 kHz of the stored events are forwarded to the High Level Triggers (HLT). The two steps of reducing this throughput of data recorded by the CMS subdetectors are described in [6] and [7] in further detail. Figure 2.6 shows a schematic overview of the trigger system.
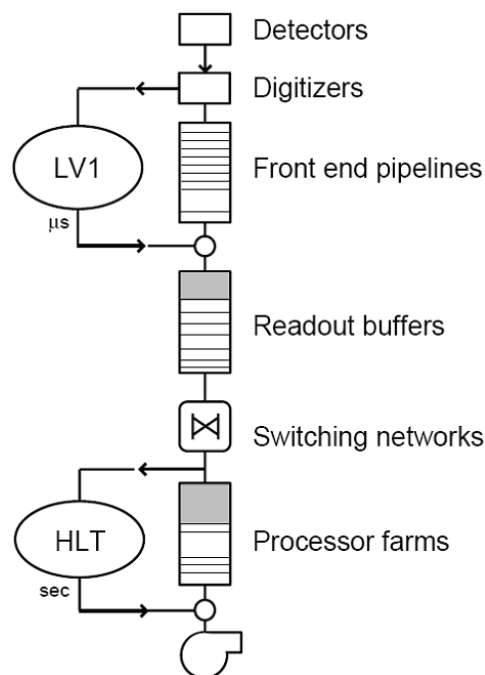
Figure 2.6: An overview of the CMS Trigger/DAQ system [7].

Level 1

The Level-1 trigger is the first step deciding whether or not to save data from the detector for each bunch crossing individually. After an interaction occurs, this decision is issued every 25ns. The pipeline data storage time for the L1 is 3.2 μs. Since this is including signal propagation delays, the L1 must often be done in less than 1 μs. If the Level-1 trigger generates an accept, the event data are read out and processed by the High Level Triggers. The L1 trigger system's decision is based on information from calorimetry and muon systems as well as some correlations of information from these systems. A diagram of the system is shown in Figure 2.7.
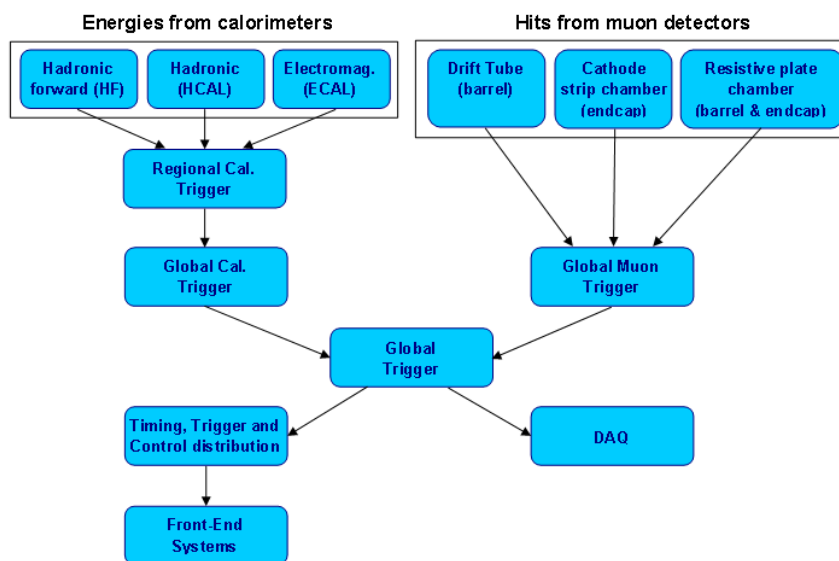
Figure 2.7: Overview of the Level-1 Trigger.

The CMS Level-1 Trigger System filters the input interaction rate of 1 GHz to an event rate of 75 kHz, which corresponds to a minimum rejection rate of 10^4 for the nominal LHC intensity.

High Level Triggers

The L1 system is based on custom electronics. By contrast, the High Level Triggers relies upon commercial processors, implemented as a processing farm. It is designed to achieve a rejection factor of 10^3, writing up to 100 events per second to mass storage. The CMS HLT/DAQ system performs the read-out of the front-end electronics after a Level-1 Trigger accept but also executes physics selection algorithms on the events read out, in order to accept the ones with the most interesting physics content. Finally these accepted events are forwarded, along with a small sample of rejected events, to the online services which monitor the performance of the CMS detector and also provide the means of archiving the events in mass storage.

2.3.2 Clock and orbit signals

Three clock and two orbit signals are provided for the experiments by the LHC machine. The frequencies of the clock signals are all around 40 MHz and the orbit frequencies are around 11 kHz (see [8] for details).

- Bunch Clock 1 (BC1): The frequency of this clock signal is connected to the bunch frequency of beam 1. For BC1 is obtained from the RF cavities accelerating the beam, its frequency value goes from 40.07888 MHz to 40.07897 MHz corresponding to the beam energies at injection (450 GeV) and collision (7 TeV).

- Bunch Clock 2 (BC2): This clock signal has the same specifications as BC1, but is bound to beam 2.

- Bunch Clock Reference (BCref): A constant frequency clock signal is fixed at the frequency value for collision (40.07897 MHz). With this, the phases of all clock signals to each other can be compared which should be constant when beam is fully ramped up.

- Orbit 1 (Orb1): This 5 ns pulse is sent out once every LHC orbit. It therefore indicates the turns making it able to keep track of individual bunches. Its period is typically 88.92us (11.246 kHz at 7 TeV), but will consequently vary as well during the ramping.

- Orbit 2 (Orb2): Behaving exactly like Orb1, it is related to the orbits of beam 2.

The *Timing, Trigger and Control* (TTC) system broadcasts these timing signals from the LHC machine to the experiments. Figure 2.8 shows the present routing of the TTC backbone. The signals are generated at the RF centre at SR4 and then sent to the *CERN Control Center* (CCC), where they are encoded to be broadcast to various destinations. The optical fibres transmitting the LHC timing signals are represented in black. The encoding, done at the CCC, is in black and grey, and the four grey lines represent the TTC signal broadcast to ALICE, ATLAS, CMS and LHCb.

Several effects such as temperature variations affect the properties of the fibre and therefore influence the phase. Measurements show that the time drift on the transmission fibres could be as large as 200 ps over a period of a day and also an annual drift of up to 8 ns has been observed (see [9]).

RF2TTC module

The most important job of the RF2TTC module is to take the optical RF signals received from SR4 and convert them into clean and stable TTC signals, which can be used by the experiments. It provides several features, such as shaping and tuning the signal outputs, all of which are remotely controllable from the network via VMEbus.

A fourth bunch clock output, BCmain, is also generated. This is basically a multiplexer between the incoming clock signals (BC1, BC2 and BCref) and an internally
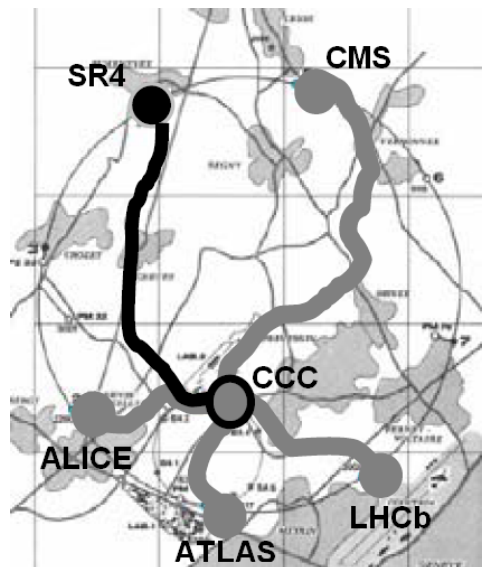
Figure 2.8: Routing scheme of the TTC backbone.

generated clock. In the same way, Orbmain is created out of Orb1, Orb2 and an internal orbit signal. The module can be set to put a delay to any of these signals in order fit the timing of the CMS subdetectors. This feature can counteract a phase drift in the clock signal driving the experiment during a run and thus allow the subdetectors to sample at the correct time. More information about the RF2TTC module can be found in [10].

2.4   Beam Pick-up Timing Experiment

1158 *beam position monitors* (BPMs) are installed around the LHC and its transfer lines to measure the position of the beam inside the pipe. The BPMs are constructed out of four electrostatic pick-up button electrodes that are built symmetrically around the beam pipe. Part of the electromagnetic field of a passing particle bunch is picked up by these detectors. By simply comparing the amplitudes of the signals coming from two opposite buttons, the beam position can be determined.

Each LHC experiment has the two BPMs next to the interaction point reserved for timing measurements, which are called *Beam Pick-up Timing Experiment* (BPTX). For CMS, the BPTX pick-ups are located 174.6 and 174.7 m away from IP5. With them, not only the timing and bunch structure of the beams coming in on either side of the experiment, but also the characteristics of individual bunches can be examined.

The BPTX is part of the CMS Beam Radiation Monitoring (BRM) system, for which a detailed description of its components and their purpose can be found in [11], [12] and [13].

2.4.1 Beam monitoring

When bunched charged particles pass a BPTX station, they cause a moving image charge travelling across the surface of the pick-ups. This image charge will give rise to a signal that will be transmitted to the CMS counting room. In the following analysis process, these signals are digitised and a software will obtain all information needed. The whole design of the beam monitoring system is described in Chapter 3, the analysis software is portrayed in Chapter 5.

2.4.2 Other CERN experiments

ATLAS

The BPTX read-out system at CMS was developed together with the *A Toroidal LHC AparatuS* (ATLAS) experiment (see [14]). A large part of the analysis software will be shared by the experiments. The flexibility of a system based on software without the need of developing new hardware is practical for both experiments, even though the requirements and software architecture are different and will lead to an independent integration of the system.

LHCb

The *Large Hadron Collider beauty* (LHCb) experiment is designed to measure the parameters of CP violation in the interactions of heavy particles containing a bottom quark, so-called b-hadrons. Dissimilar to CMS and ATLAS, its system to read-out and analyse the BPTX signals is hardware based. The beam monitoring system is built around a custom made electronics board, which enables real-time bunch monitoring. Real-time measurements will be stored for each bunch by writing the phase and intensity into the event data stream (see [9] for more details).

ALICE

The *A Large Ion Collider Experiment* (ALICE) will study heavy ion collisions. When colliding Pb-Pb nuclei with a centre of mass energy of 5.5 TeV per nucleon, the resulting temperature and energy density will generate a quark-gluon plasma. This is a state of matter wherein quarks and gluons are deconfined. For monitoring the beam, ALICE will probably use an LHCb-like solution.

Chapter 3

Design of the beam monitoring system

The ability to detect the times when the bunches come into the experiment is a vital necessity when timing the subdetectors at CMS. This has to be done so that the correct phase to sample the data can be found. Unfortunately, once the timing of subdetectors is set, the phase of the clock signals may drift due to various unforeseen reasons (e.g. temperature changes, see Section 2.3.2). This could make the data recording for the experiment very poor. Therefore, the primary purpose of a beam monitoring system is to provide this timing reference and to monitor any drifts in the timing signals in order to compensate for them in other subsystems.

The monitoring of the beam structure of the two particle beams is the second purpose. The signals coming from the BPTX detectors hold information about the intensities and lengths of the individual bunches as well as the filling patterns of the beams. Satellite or ghost bunches of significant size can also be detected by examining the BPTX signals.

3.1   Requirements

The following list states all tasks to be performed and requirements to be fulfilled and also the frequency with which these should be executed.

1. Phase: The phase between each bunch and the corresponding clock/orbit tick is measured to a precision less than 100 ps (once a minute).

2. Intensity, length: The intensity and length of each bunch is measured (once a minute).

3. Bunch pattern: The correctness of the filling scheme and whether the position of each bunch is in the right RF bucket is checked (once a minute).

4. Ghost bunch: The presence of ghost bunches in neighbouring RF buckets is checked (once a minute).

5. Clock: The quality of the clocks is measured, i.e. frequency, cycle duration, duty cycle, jitter of individual clock signals and also phases between clock signals (once a minute).

6. Orbit: The quality of the orbits is measured, i.e. frequency, cycle duration, duty cycle, jitter of individual orbit signals and also phases between the two orbit signals and between orbit and corresponding BPTX/clock signals (once a minute).

7. Data storage: The data of all measurements should be time-stamped with a precision of the order of seconds, published with a delay of less than a minute and stored in a retrievable way.

8. Configuration: The beam monitoring system should configure itself automatically, especially the sensitivity of the inputs should match the strength of the BPTX and clock/orbit signals automatically.

3.2   Idea and choice of technology

For LHC is still under construction and also unknown issues could come up during operation, CMS has chosen to use a flexible solution to be able to adapt to all needs becoming apparent. Figure 3.1 shows an overview of how CMS will use the BPTX detectors.
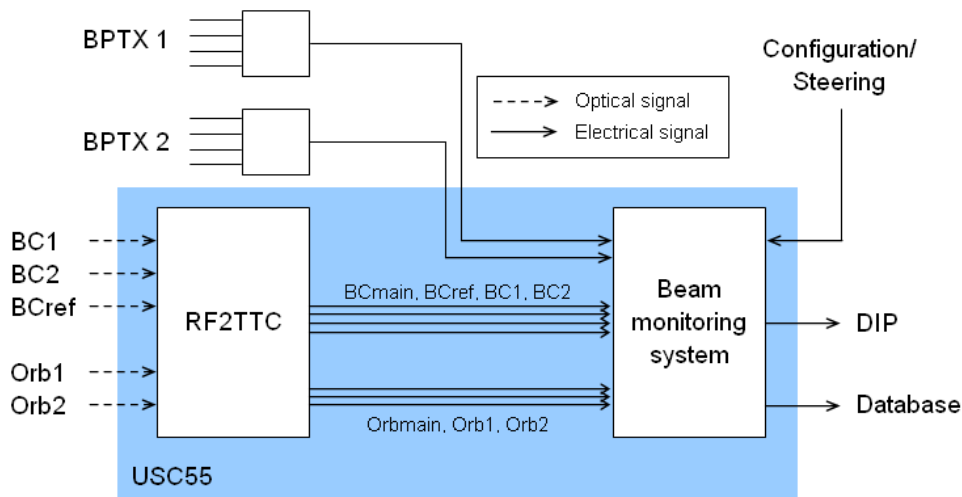
Figure 3.1: Block diagram of the beam monitoring system showing how CMS will use the various signals.

At each BPTX pick-up station the voltage from all four button electrodes is added up. After travelling through over 200 m cable, these sum-signals end up in an electronics rack in USC55 and are an input to the beam monitoring system. The other inputs, various clock and orbit signals, are first converted from optical signals and shaped in the RF2TTC board before reaching the beam monitoring

system. Furthermore, the system will get information from the LHC machine, i.e. its running mode, beam intensities, running energies, etc. This information is used to calculate the expected signal amplitudes and filling schemes which are then used as a reference while running the analysis.

The monitoring information resulting from the analysis will be stored permanently in an CMS database. Since some data is also useful for other parts of the experiment it will also be published via *Data Interchange Protocol* (DIP).

The beam monitoring system is split up in two main parts, hardware for data acquisition and software for data analysis. The data acquisition will be realised with commercial digital sampling oscilloscopes, since they meet the high demand in flexibility and debugging possibilities. Using their analog-to-digital conversion and network communication features, the data can be easily read out by any computer. The analysis software can also be written in any programming language, thus providing a user-friendly interface and an ability for integration and communication with other systems. Moreover, quick alterations and adjustments of the software algorithms are possible.

Before the analysis software can be designed, the signals coming from the pick-up stations need to be understood and able to be modeled. Then, the analysing algorithms can be developed. Chapter 4 will discuss the BPTX signal in detail and Chapter 5 will deal with design of the software.

Chapter 4

Signal from the beam pick-up detectors

In order to obtain all information needed about the particle beams, the characteristics of the expected BPTX signal need to be foreseen. Therefore, thorough calculations are needed. Furthermore, the hardware for the data acquisition is selected according to the maximum signal amplitude. Thus, in the following chapter a model is derived for a signal produced by a passing particle bunch. Afterwards the effects of a 200 m cable on the signal measured by an oscilloscope are taken into account. Finally the signal characteristics for various beam scenarios is are calculated.

4.1   Operating principle of pick-ups

So-called Beam Position Monitor (BPM) stations are installed around the accelerator ring to constantly monitor the transverse beam position inside the beam pipe. Each station consists of four button pick-ups, which are mounted around the beam pipe symmetrically. The pick-up signal varies linearly with the beam distance for small position deviations from the centre. When comparing the amplitude ratios of opposite buttons, the beam position inside the pipe can be determined. The BPTX stations are built similarly and mounted 175 m away from the interaction point. The sum of the signals from all four buttons is approximately independent of the traverse beam position. The signals from all four pick-ups are therefore added to keep the signal constant, even for small deviations.

The pick-ups in the BPTX stations are so-called electrostatic button electrodes. The working principle is based on simply picking up a part of the electromagnetic field created by the passing particle bunches. These particle bunches are charged and give therefore rise to an electromagnetic field when circulating in the LHC. The positively charged bunches cause the free moving electrons of the metallic beam pipe to form a mirror charge on its surface. This mirror charge follows the bunches around the accelerator, thus producing a mirror current with equal magnitude but opposite sign compared to the bunch current. When travelling across the circular surface of the button pick-up electrode, the image current creates a signal. The particle beams are not influenced by the BPTX monitoring, because the energy of

this pick-up signal is negligibly small compared to the beam energy.

This working principle including the relativistic effects on the field is discussed in more detail in [15].

4.2 Calculations

In order to describe the mathematical model of the bunches and the resulting signals, the co-ordinate system has to be defined first. The origin is in the centre of the pick-up, i.e. the measurement point. The z-axis will along the direction of the beam. The x-axis will then be set to point away from the centre of the earth and the y-axis is therefore set along the radial direction of the accelerator. Depending on the direction of the beam, the y-axis will be either pointing inwards or outwards. Thus, a right-handed Cartesian coordinate system is set up.

4.2.1 Particle bunch model

At normal intensity an LHC bunch will contain $1.15 \cdot 10^{11}$ protons. As this bunch is accelerated around the ring it will have a transversal footprint of a few hundred μm, which at the inter-action point is focused down to 16 μm. Even with the longitudinal grouping of the bunch by the sinusoidal accelerating field, the protons are spread out along the z-axis. This linear charge distribution can be approximated with a Gaussian function, where the standard deviation σ_z can be used as a measure of the length of the bunch. According to [16], this bunch will be 7.55 cm at the collision energy of 7 TeV, which corresponds to 252 ps when measured in the reference frame of the laboratory. With this approximation an expression for the linear charge density for a bunch centred around $z = 0$ can be stated.

$$\rho\left(z\right) = \frac{Ne}{\sigma_z\sqrt{2\pi}}e^{-\frac{z^2}{2\sigma_z{}^2}} \tag{4.1}$$

The area under the curve must equal to the total charge of the bunch. Therefore, equation 4.1 is normalised with the number of protons N and the proton charge e.

Since the bunches move around the accelerator with a velocity v close to the speed of light, changing z for $z - vt$ in equation 4.1 results in the description of the charge collected on the beam pipe at any given point and time.

$$\rho\left(z, t\right) = \frac{Ne}{\sigma_z\sqrt{2\pi}}e^{-\frac{(z-vt)^2}{2\sigma_z{}^2}} \tag{4.2}$$

Figure 4.1 shows the linear charge density function of a single bunch at $t = 0$ for nominal LHC intensity at injection and at collision.

4.2.2 BPTX signal model

The centre of the pick-up is set to be $z = 0$ and $t = 0$ is the time when the centre of the bunch passes this point. Furthermore, it is assumed that the beam can be considered as an ideal current source, when moving the image charge on the surface
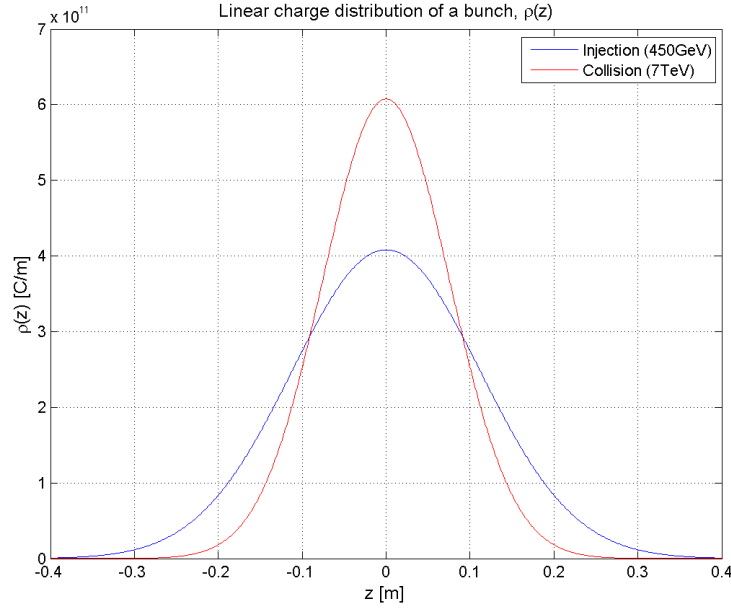
Figure 4.1: The linear charge distribution of a single bunch.

of the beam pipe. Therefore, the charge distribution on the pipe will be of opposite sign but equal magnitude.

Since this charge density will be spread out evenly on the beam pipe inside, the charge collected on a pick-up button at a certain z-value depends on its angular coverage of the beam pipe circumference c_{ang}. Only considering the x-z-plane, for each point on the button circumference

$$x^2 + z^2 = r_b{}^2 \implies x = \pm\sqrt{r_b{}^2 - z^2} \tag{4.3}$$

holds true, where r_b is the radius of the button electrode. The ratio of the circumference of the beam pipe covered by the pick-up can then be stated as

$$c_{ang}(z) = \frac{\sqrt{r_b{}^2 - z^2}}{\pi r_{pipe}} \tag{4.4}$$

where r_{pipe} is the radius of the beam pipe. Figure 4.2 shows this geometrical factor for the case of the BPTX station at CMS, where the radius of the button pick-up is 17 cm and the radius of the beam pipe equals 31.5 cm.

When integrating the linear charge density multiplied by the button angular coverage over z, one gets the charge collected on the button at time t.

$$Q_{img}(t) = \int \rho(z,t)\, c_{ang}(z)\, dz \tag{4.5}$$

The current on the button is found by differentiating equation 4.5 with respect to time.

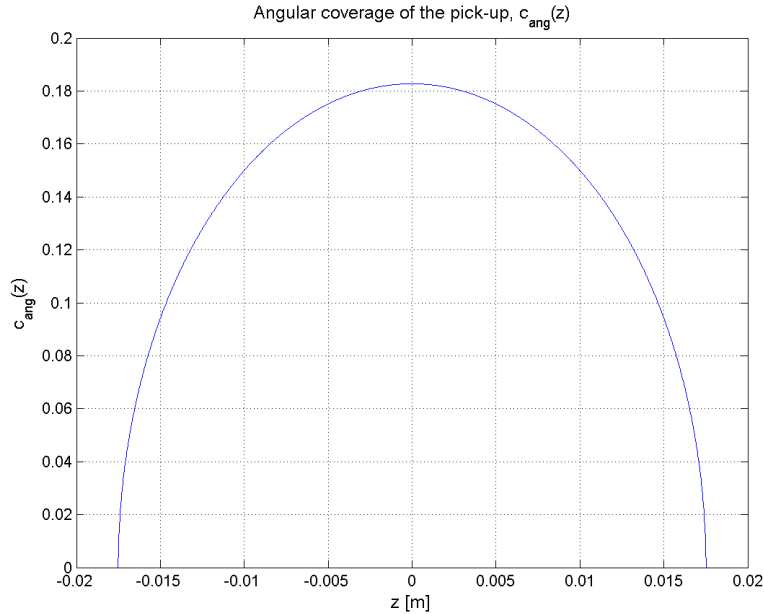$$i_b(t) = \frac{dQ_{img}(t)}{dt} \tag{4.6}$$

Figure 4.2: The angular coverage of the pick-up electrode.

Since only the charge density is time dependent, this can be written as

$$i_b(t) = \int \frac{\partial \rho(z,t)}{\partial t} c_{ang}(z)\, dz \tag{4.7}$$

$$i_b(t) = \frac{Nev}{r_{pipe}\sigma_z{}^3\pi\sqrt{2\pi}} \int (z-vt)\, e^{-\frac{(z-vt)^2}{2\sigma_z{}^2}} c_{ang}(z)\, dz \tag{4.8}$$

Figure 4.3 shows a time-discrete representation of the button current for the two key energies.

In order to calculate the button voltage, the impedance of the button needs to be determined. It consists of the impedance of the coaxial cable R_{coax} in parallel with the capacitance between beam and button electrode C_b.

$$Z_b(\omega) = \frac{1}{\frac{1}{R_{coax}} + \imath\omega C_b} \tag{4.9}$$

The real and imaginary parts of Z_b are plotted in Figure 4.4. R_{coax} was given by the datasheet to be 50 Ω (see [17]) and C_b was measured to be 16.09 pF (see [18]).

By taking the inverse Fourier transform of the impedance in equation 4.9, one gets the impulse response of the button electrode (see Figure 4.5).

$$z_b(t) = \mathcal{F}^{-1}\{Z_b(\omega)\} \tag{4.10}$$

$$z_b(t) = \frac{1}{C_b} e^{-\frac{t}{R_{coax}C_b}} \tag{4.11}$$

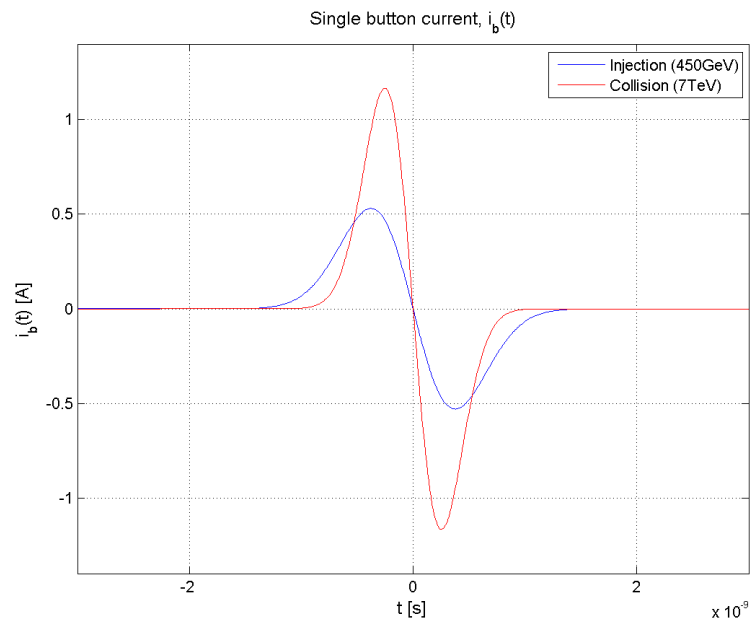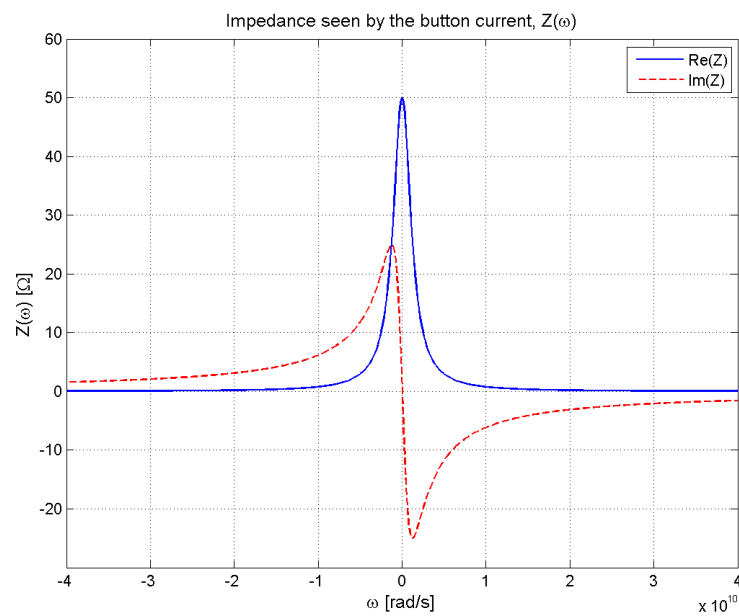**Figure 4.3:** The current on a single button caused by a passing bunch.

Figure 4.4: Impedance seen by the button current.

The input signal to this system is the button current $i_b(t)$ and the output signal is the button voltage $u_b(t)$. To obtain the output signal, the impulse response is sampled with the same sampling frequency as the current and a discrete convolution of the two signals is calculated.
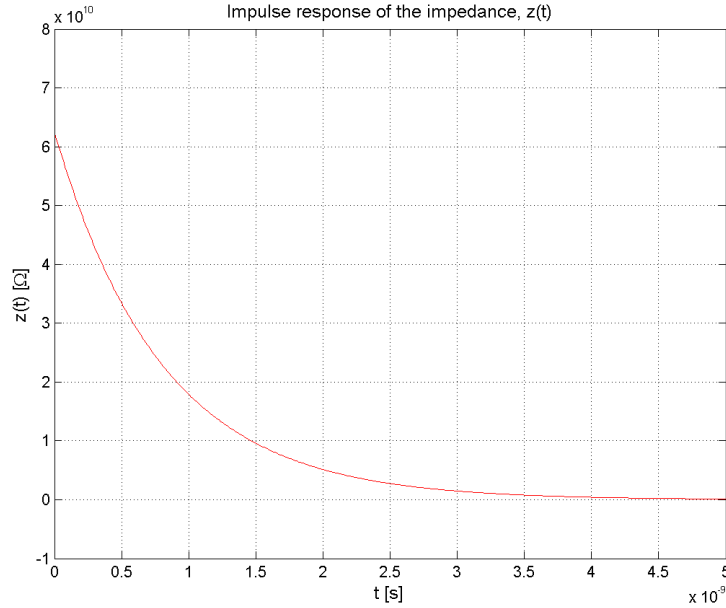
Figure 4.5: Impulse response of the impedance.

$$u_b(t) = (z_b * i_b)(t) \tag{4.12}$$

$$u_b(t) = \int z_b(t_0) i_b(t - t_0) dt_0 \tag{4.13}$$

The resulting button voltage is plotted in Figure 4.6. A closer look at $u_b(t)$ shows that the signal is closely related to the derivative of the charge distribution, but distorted by the frequency dependency of the parasitic capacitance between the beam pipe and the button electrode.

The frequency spectrum of the voltage signal at the pick-ups can be determined by performing a Fourier transform (see Figure 4.7).

$$U_b(\omega) = \mathcal{F}\{u_b(t)\} \tag{4.14}$$

4.2.3 Transmission line effects

The effects of the 200 m cables installed between the CMS BPTX stations and the rack in the CMS underground counting room USC55 are not negligible. The data sheet for the Nexans CMA 50 cables states the attenuation factors for a few frequency values (see Appendix A for more details and also how the cable lengths were measured).

To build a more general model of how the attenuation factor depends on frequency, a continuous function was fitted to the points in the data sheet. The exponential function in Eq. 4.15 fits the data points very well and is plotted in Figure

Figure 4.6: Voltage from a single button.

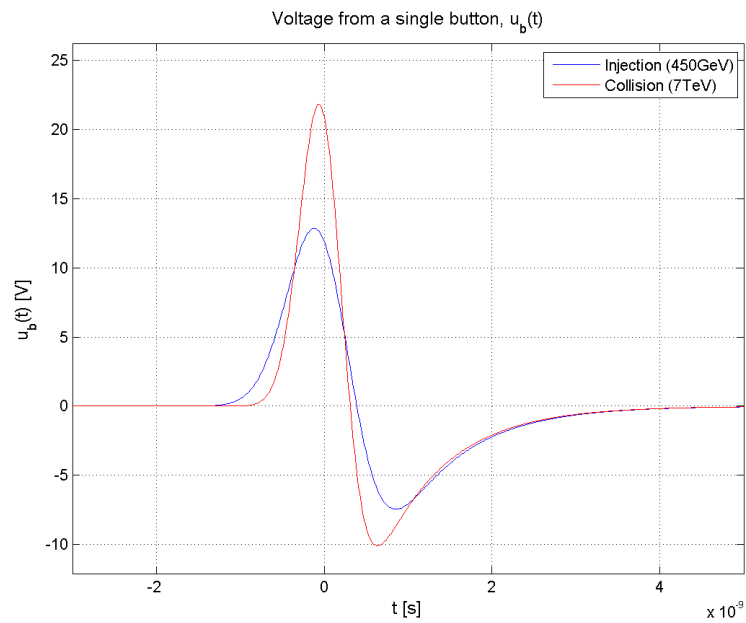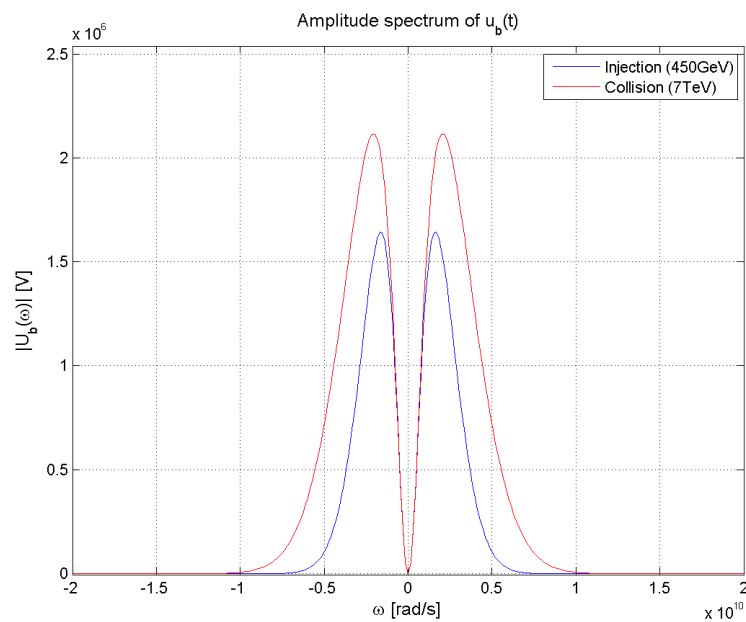**Figure 4.7:** Amplitude spectrum of u_b.

4.8.

$$a_{cable}\left(\omega\right) = 0.6470 \cdot e^{-3.1658\cdot10^{-10}\omega} \tag{4.15}$$

The signal after the transmission line is now readily determined by multiplying
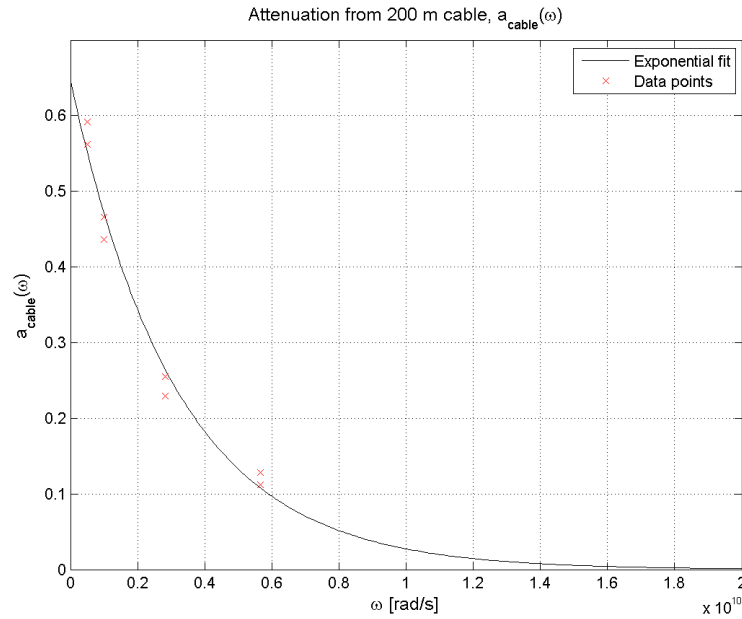
Figure 4.8: Cable attenuation.

each frequency in $U_b(\omega)$ with its corresponding cable attenuation.

$$U_{b,cable}(\omega) = U_b(\omega) \cdot a_{cable}(\omega) \tag{4.16}$$

Figure 4.9 shows the frequency spectrum of the signal after the cable is taken into account $U_{b,cable}(\omega)$. A shift in location for the bulk of the signal is to be expected along with a very large over-all attenuation, which can be seen in Figure 4.10.

$$u_{b,cable}(t) = \mathcal{F}^{-1}\{U_{b,cable}(\omega)\} \tag{4.17}$$

4.2.4 Oscilloscope bandwidth effects

The last effect which has to be taken into consideration in these calculations is the limited bandwidth of the oscilloscope. The oscilloscope has a high-frequency cut-off which is defined as the frequency at which a sinusoidal input signal is attenuated to 70.7% of the signal's true amplitude, known as the -3dB point. The frequencies below this cut-off are well recorded while frequencies above this value are heavily attenuated. Therefore, the effects of the limited bandwidth of the scope can be modeled by a low-pass filter. By letting ω_{BW} symbolize the high-frequency cut-off of the oscilloscope bandwidth in rad/s and using a standard filter model (see [19]) transfer function of the filter $H_{scope}(\omega)$ can be written as in Eq. 4.18. The frequency-response curve of the oscilloscope attenuation can be seen in Figure 4.11.

$$H_{scope}(\omega) = \frac{1}{1 + i\frac{\omega}{\omega_{BW}}} \tag{4.18}$$
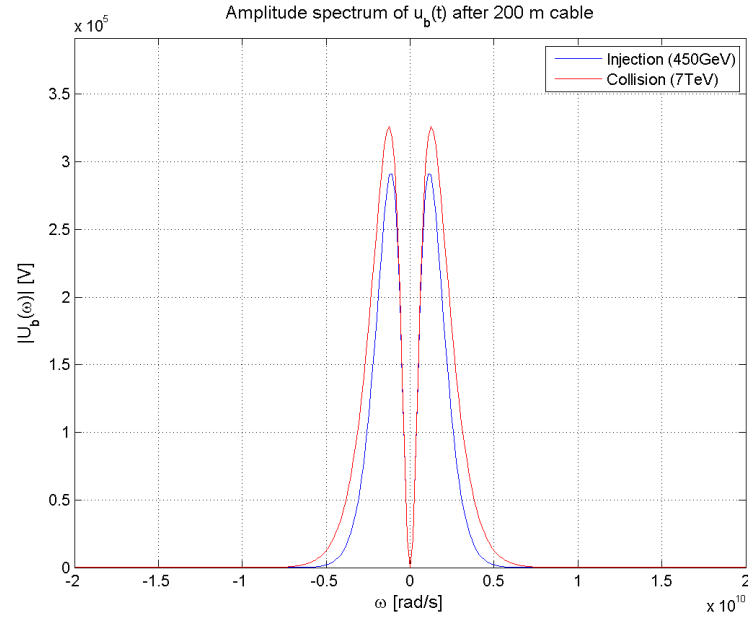
Figure 4.9: Amplitude spectrum of u$_b$ after cable.
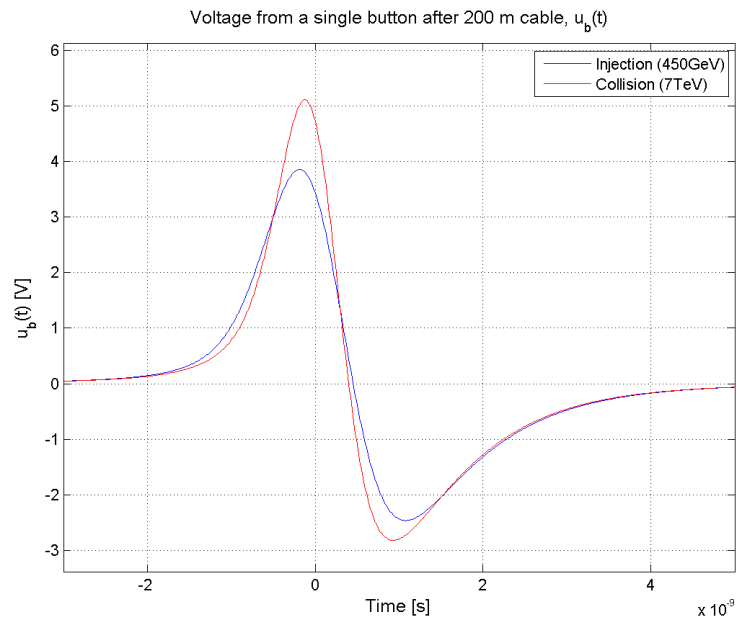
Figure 4.10: Voltage from a single button after cable.

By multiplying $U_{b,cable}(\omega)$ with the attenuation, the effects of the oscilloscope bandwidth are taken into account. The resulting frequency spectrum $U_{b,scope}(\omega)$ represents the signal expected for a typical LHC bunch after the transmission line and the limited bandwidth of the oscilloscope have been considered. The effects on
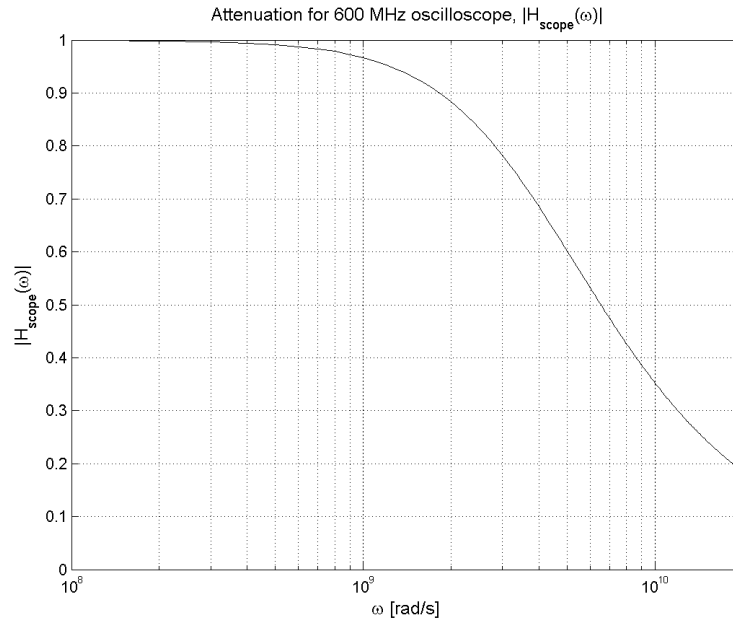
Figure 4.11: Scope attenuation.

the spectrum of the signal is shown in Figure 4.12.

$$U_{b,scope}\left(\omega\right) = U_{b,cable}\left(\omega\right) \cdot H_{scope}\left(\omega\right) \tag{4.19}$$
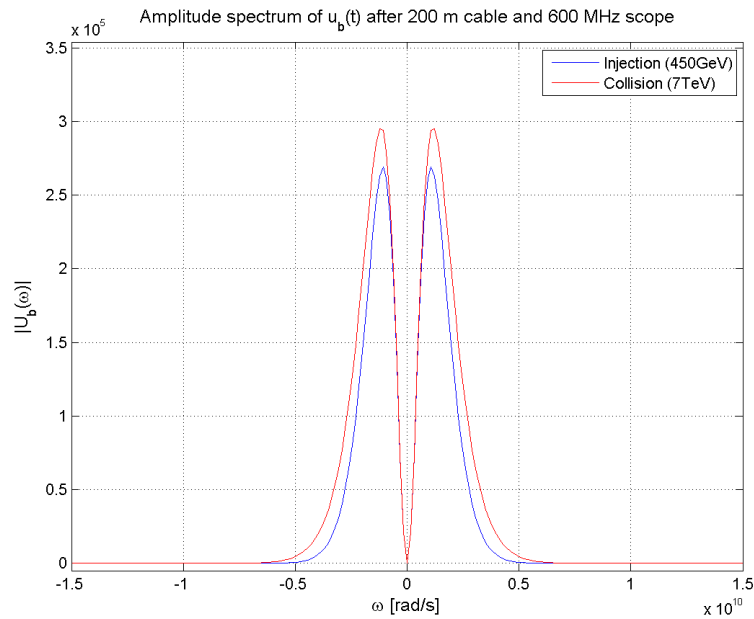
Figure 4.12: Amplitude spectrum of u$_b$ after cable and scope.

Figure 4.13 shows the signal after both cable and oscilloscope.

$$u_{b,scope}(t) = \mathcal{F}^{-1}\{U_{b,scope}(\omega)\} \tag{4.20}$$
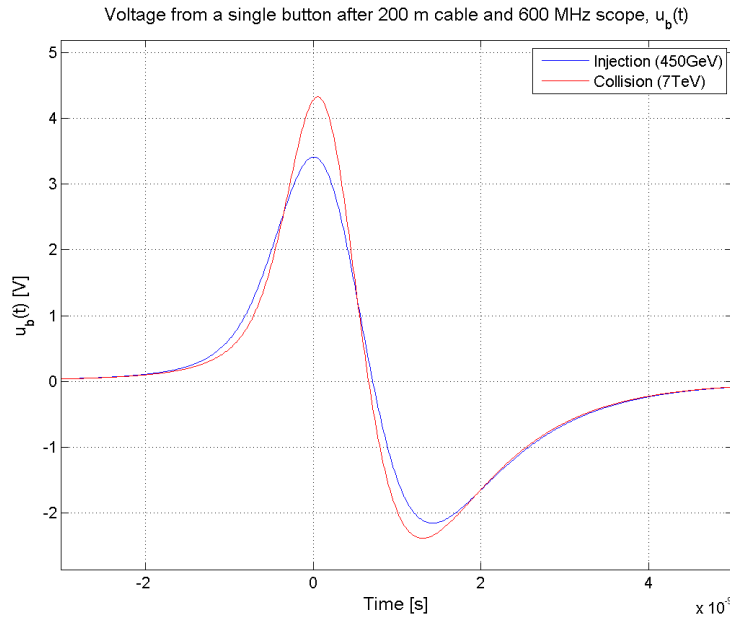
Figure 4.13: Voltage from a single button after cable and scope.

Figures 4.14 and 4.15 compare the amplitude spectrum and the voltage from 4 buttons. Thus, the effects of the different parts of the system on the signal can be studied. These plots were generated assuming a typical LHC bunch with $N = 1.15 \cdot 10^{11}$ and $\sigma_z = 0.075$ m at 7 TeV.

4.3   Dependency on bunch parameters

Now that a complete model for the BPTX signal has been formed,

$$U_{b,final}(\omega) = U_b(\omega) \cdot a_{cable}(\omega) \cdot H_{scope}(\omega) \tag{4.21}$$

$$u_{b,final}(t) = \mathcal{F}^{-1}\{U_{b,final}(\omega)\} \tag{4.22}$$

it is possible to study how the signal shape and amplitude varies with the bunch intensity and length. Since the number of protons, N, only appears as a scale factor in the expression for the button current $i_b(\omega)$ this dependency is trivial (see Eq. 4.8). It is harder to predict how the signal shape and amplitude will be affected by different bunch lengths. A longer bunch length will spread out the signal, but it is not obvious how the shape changes.

Since the data acquisition hardware can be damaged by high voltage peaks, it is useful to see exactly how the signal scales for different values of the bunch length σ_z.
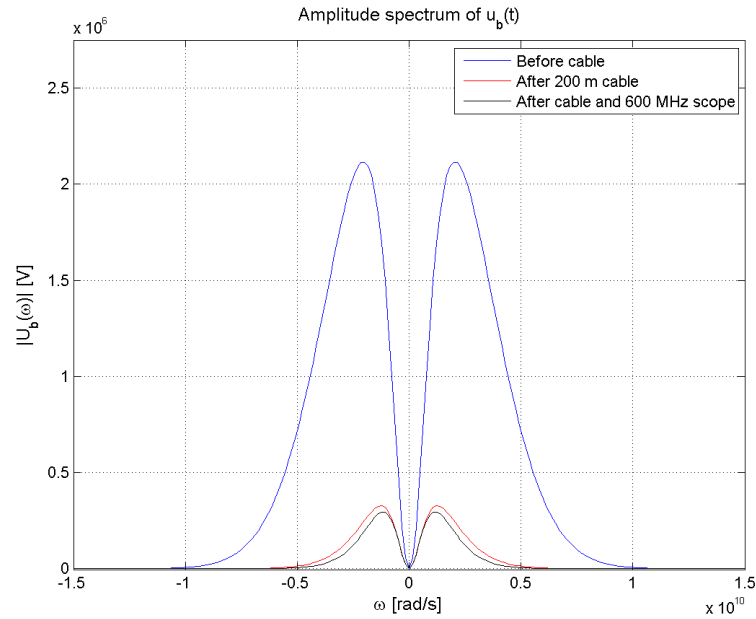
Figure 4.14: Amplitude spectrum of u_b at the electrode, after the cable and with the effects of the oscilloscope
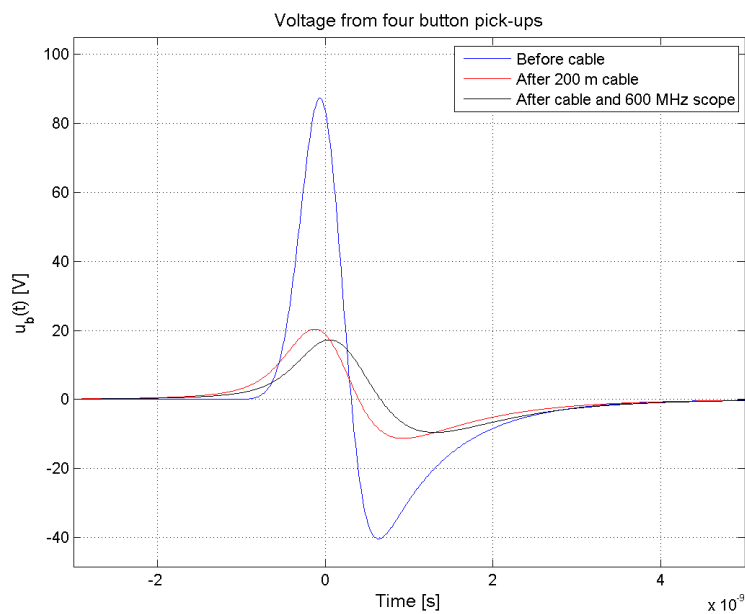
Figure 4.15: Voltage from 4 buttons at the BPTX station, after the cable and with the effects of the oscilloscope.

To gain understanding about how the bunch length affects the maximum amplitude of the peak in the bipolar pulse, the distance from signal peak to valley and the area under the positive half of the curve, Figure 4.16 - 4.18 were generated. These

three values are not directly proportional to the bunch length, but vary in a more complex way. However, since a signal caused by a longer bunch has a smaller spread in frequency space, it is attenuated less by the cable. This causes the relations to be almost linear in the interesting interval.
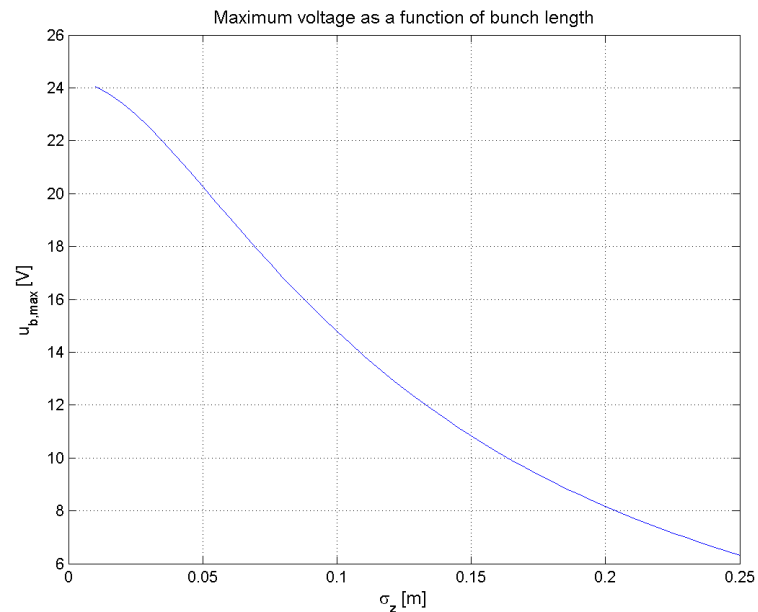
Figure 4.16: Maximum voltage as a function of bunch length.
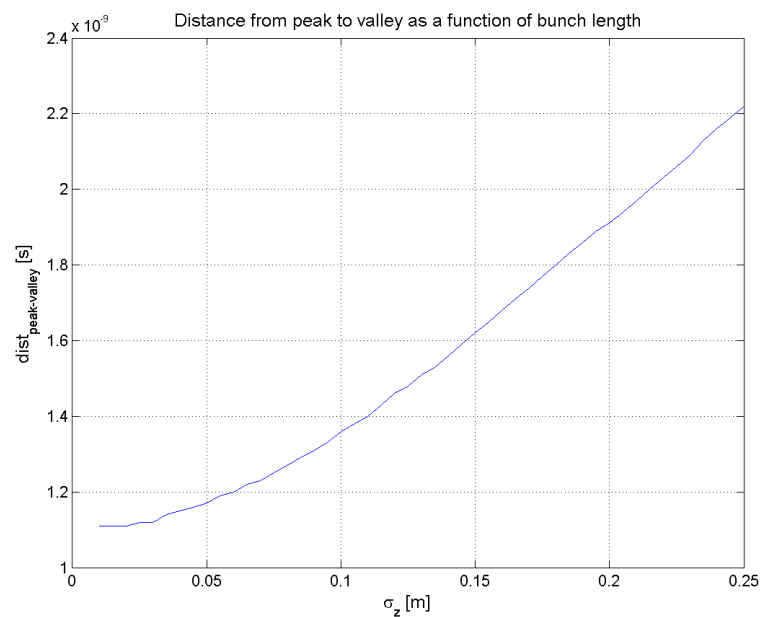
Figure 4.17: Distance from peak to valley as a function of bunch length.
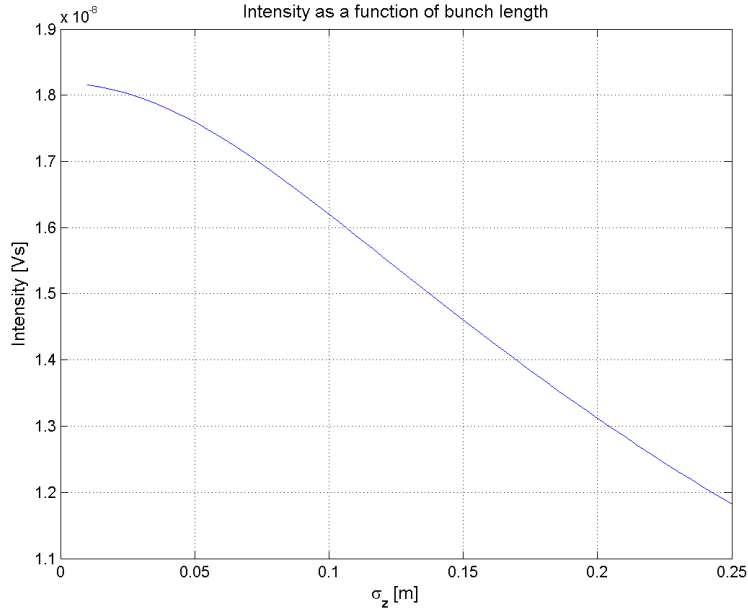
Figure 4.18: Intensity as a function of bunch length.

4.4   Beam scenarios

Since the LHC beam energy goes from 450 GeV at injection to 7 TeV at collision, the RMS bunch length for the Gaussian linear charge distribution varies from 11.24 cm down to 7.55 cm, which corresponds to 375 ps at injection and 252 ps at collision. Table 4.1 shows intensities and bunch spacings for the different beam scenarios.

Table 4.1: LHC proton parameters for various scenarios (see [16]).

	Pilot	Commissioning	First Year	Nominal	Ultimate
# of bunches	1 - n.a.	44	2808	2808	2808
# of particles per bunch	$5.00{\cdot}10^9$	$1.15{\cdot}10^{11}$	$4.00{\cdot}10^{10}$	$1.15{\cdot}10^{11}$	$1.67{\cdot}10^{11}$
Bunch spacing [ns]	n.a.	2021	24.95	25	24.95

With these parameters the expected signal can be calculated Using Eq. 4.21 and 4.22 (see Table 4.2). The result for the distance between peak and valley of the bipolar pulse is not dependent on the number of particle per bunch and is therefore the same for all scenarios, i.e. 1.41 ns at injection and 1.25 ns at collision. Since the final read-out for the CMS BPTX will be based on the LeCroy WR64Xi oscilloscope with a bandwidth of 600 MHz and the BPTX cable at point 5 is about 200 m long, the values in Table 4.2 were calculated taking these effects into account. It can can be seen, that the numbers in the table imply a maximum voltage range of about factor 50 in voltage.

Figure 4.19 compares the voltages from four buttons after 200 m cable and taking the effects of a 600 MHz scope into account.

Table 4.2: Expected maximum and minimum voltage, resulting signal range and area the under positive half of the curve for various beam scenarios.

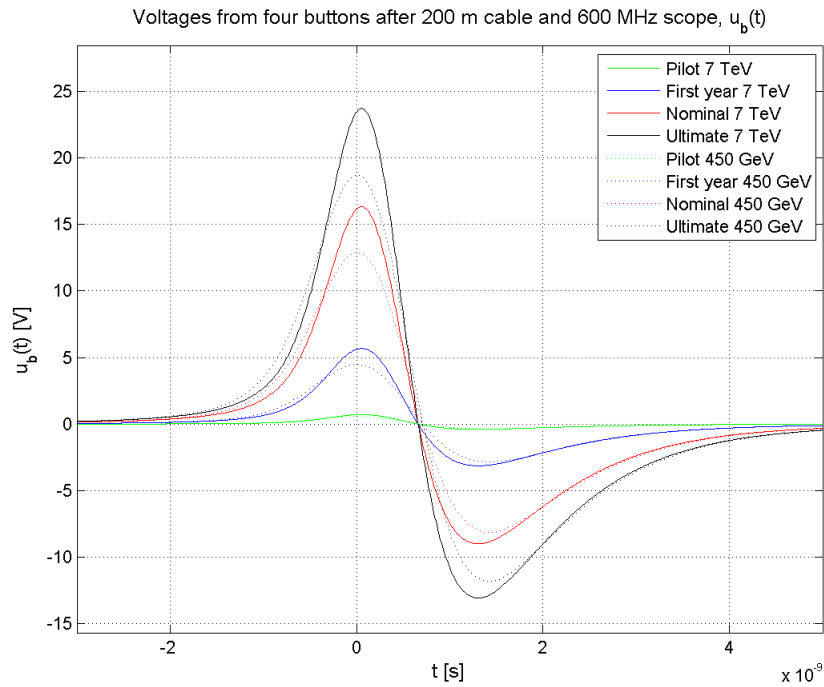|	Pilot		First Year		Nominal		Ultimate	
	450 GeV	7 TeV	450 GeV	7 TeV	450 GeV	7 TeV	450 GeV	7 TeV
Maximum [V]	0.56	0.71	4.48	5.68	12.88	16.32	18.70	23.70
Minimum [V]	-0.35	-0.39	-2.83	-3.13	-8.13	-8.99	-11.80	-13.06
Range [V]	0.91	1.10	7.31	8.80	21.01	25.31	30.51	36.76
Pos. area [Vs]	$6.47{\cdot}10^{-10}$	$6.94{\cdot}10^{-10}$	$5.18{\cdot}10^{-9}$	$5.56{\cdot}10^{-9}$	$1.49{\cdot}10^{-8}$	$1.60{\cdot}10^{-8}$	$2.16{\cdot}10^{-8}$	$2.32{\cdot}10^{-8}$

Figure 4.19: Comparing the bipolar bunch signals for various beam scenarios after 200 m cable and the effects of a 600 MHz scope.

Chapter 5

Design of the data analysis software

The software analysing the BPTX signals was designed like a kit of building blocks. This modular conception provides for an easy exchange of analysis algorithms, a user interface, signal acquisition, data storage, etc. The various blocks can be used to put together small analysis programmes for implementation and testing purposes. Basic and adaptable data structures are applied to support this flexibility.

5.1   Design overview

The programming language LabVIEW by National Instruments was chosen for the implementation of the beam monitoring software. LabVIEW's main advantages are its strong features in measurement automation and signal processing, which makes it very suitable for the BPTX read-out. Furthermore, with its built-in functions the data acquiring hardware can be remotely controlled via standard communication protocols. User interfaces and data displays can also be realised in a quick and easy way.

The flow chart in Figure 5.1 shows the various software components and the data types they exchange with each other. The first step of the analysis is accomplished by the *waveform processors*. These modules process the signal waveforms sample by sample, thus extract interesting information and save the result in a *waveform descriptor*. Combining the waveform descriptors from BPTX, clock and orbit signals, each bunch is related with a phase and a *Bunch Crossing Identifier* (BCID) by the *Phase & BCID associator*. The database is used to store all results with a time stamp. An in-depth description of the software blocks and data structures is given in Section 5.3.

5.2   Required features

The following specifications of the software can be formulated, based on the system requirements stated in Section 3.1.

1. Phase, BCID: The phase of each bunch with respect to the clock signal is to be calculated. Furthermore, each bunch is to be given a BCID to identify its position in the bunch train.
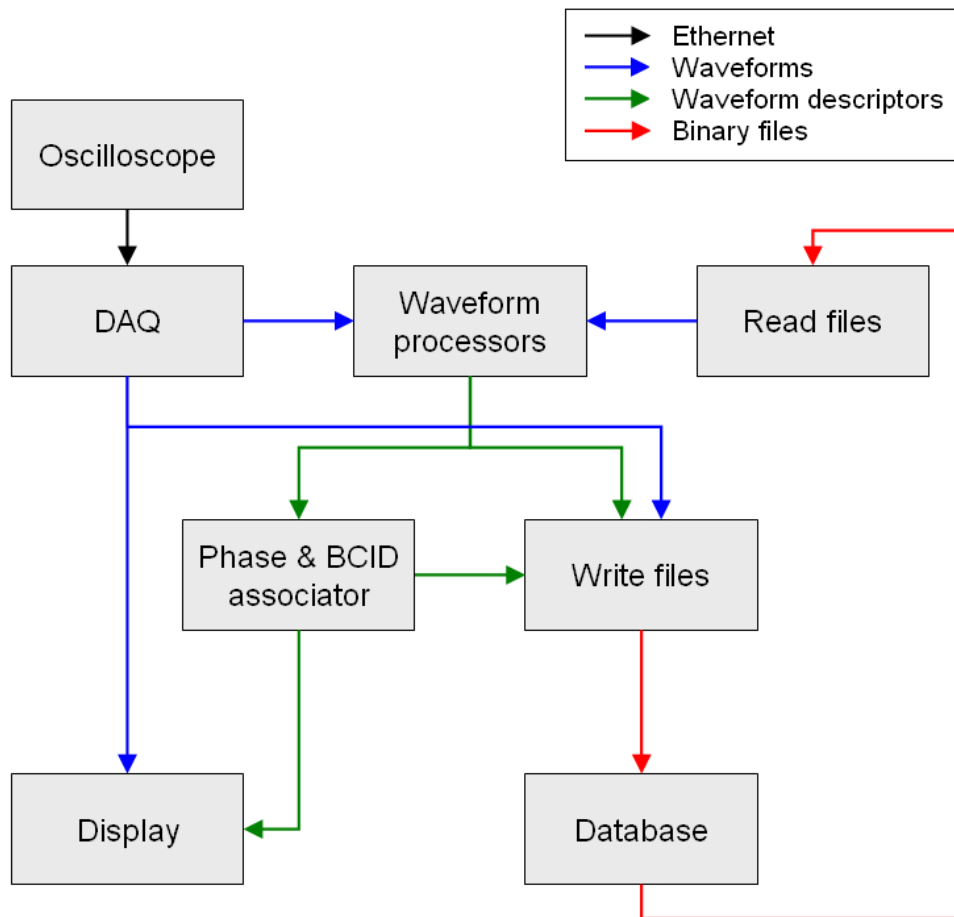
Figure 5.1: This chart shows the communication flow of the different software components.

2. Intensity, length: The intensity and length of each bunch is to be measured every acquisition.

3. Bunch pattern: The agreement of the actual LHC filling scheme with the expected one is to be verified.

4. Ghost bunch: Satellite bunches above noise level are to be identified.

5. Clock: The frequencies and jitters of the clock signals are to be checked.

6. Orbit: The frequencies and jitters of the orbit signals are to be checked.

7. Data storage: Information is to be extracted from the measurements and saved with a time stamp.

8. Display: Relevant data is to be presented in a clearly structured and detailed way.

9. Stability: The algorithms analysing the signals are to be programmed to process even the most abnormal input data without causing a system failure.

5.3   Data structures

5.3.1   Waveform

The actual signal is recorded by the oscilloscope by storing a binary representation of all sample points. The data structure is explained in Table 5.1.

Table 5.1: Contents of the data structure *waveform*.

Name	Data type	Description
t_0	Time stamp	Time when the waveform acquisition is started with respect to the trigger.
dt	Double	Time between the sample points, given in nanoseconds.
Y	$1 \times n$ array of doubles	Sampled signal values.

5.3.2   Waveform descriptor

The waveform processors analyse the signal waveform and extract all desired information, which is then put into a so called *waveform descriptor*. This data type is the compressed representation of the signals containing various parameters describing the waveform. The same data format is used for BPTX, clock and orbit types. Thus, a very flexible data structure had to be implemented (see Table 5.2).

Table 5.2: Contents of the data structure *waveform descriptor*.

Name	Data type	Description
Signal type	String	Type of signal which the descriptor contains (e.g. "BPTX1", "BC2", "Orb1", etc.).
Time stamp	Time stamp	Time between when the waveform was acquired and January 1st 1904, 12:00 (Universal Time), given in seconds.
Property names	$1 \times n$ array of strings	Names of the properties (e.g. "Length", "Intensity", "Positive edge", etc.).
Property data	$m \times n$ array of doubles	Values of the n parameters for m identified features (e.g. bunches or clock ticks).

When the bunch signal processor analyses a BPTX signal, it extracts all parameters which describe the bunches and places them in such a data structure. By simply expanding it, the phases of the bunches and their BCIDs, computed by the Phase & BCID associator, can be added. If this data structure is used to store information extracted from a BPTX acquisition, it is called a *Bunch Train Descriptor* (BTD). Otherwise (i.e. when saving information from clock or orbit signals) it is called a *Square Pulse Train Descriptor* (SPTD).

5.4   Data acquisition

Stability and efficiency are the most important requirements for the data acquisition (DAQ). LabVIEW includes a broad range of support for communication with DAQ hardware, such as an oscilloscope. However, oscilloscope-specific drivers had to be integrated into the software.

5.5   Waveform processors

The following sections introduces the methods and algorithms for extracting parameters which describe the bunches and clock/orbit ticks in the signals acquired with the oscilloscope.

5.5.1   Bunch signal processor

Knowing of how bunch characteristics affect the BPTX signal pulses, as described in Chapter 4, algorithms can be designed to go backwards, i.e. extract information about the bunches by examining the BPTX signal. As discussed, the bunches can be described by three parameters. The arrival time t_0 indicates when a bunch passes the pick-up, intensity N holds information about the number of particles in the bunch and length σ_t describes the longitudinal spread of the bunch.

The signals from the BPTX pick-ups are very complicated to analyse. The easiest method to extract the bunch parameters, namely cutting out a window around the bipolar pulse and fitting a model function to it, needs a lot of calculation and therefore slows the system. Thus, other measures of the bunch properties must be defined, since a balance between processing speed, good parameter measures and accuracy has to be found for the final system.

Arrival time t_0

Finding the point in time when the bipolar signal crosses zero was found to be the best way to determine the bunch location in the captured bunch train (see Figure 5.2a). The time when a certain threshold is crossed or the location of the signal peak depend too much on the signal intensity and length, therefore making it inappropriate for timing purposes. The zero-crossing will not move much for bunches of different lengths and intensities. It is also the steepest part of the signal which increases the resolution even more.

The simplest way to obtain this value is to form a straight line between the smallest positive and negative sample points between the peak and the valley, and then determine the zero-crossing of this line. For the final implementation of the system, there will be an offset which needs to be calibrated and corrected for in the system.

Bunch intensity N

The amplitude of the signal (see Figure 5.2b) is not a good measure of the bunch intensity, since it is also dependent on the bunch length. An increase of the beam energy will cause a longitudinal contraction of the bunch and therefore also lead to a higher amplitude. Integrating the signal is an alternative to overcome this problem, since a shorter but higher pulse would result in the same area. However, the negative part of the bipolar signal shows a long tail and is therefore difficult to have integration limits assigned. Thus, only the area under the peak is summed up. In this case, the lower integration limit is a threshold-crossing and the upper limit is the zero-crossing (see Figure 5.2c).

Integrating only the peak of the signal makes the analysis also less sensitive to ghost bunches. These are most likely to appear in neighbouring RF buckets (i.e. at least 2.5 ns away). Because the negative bunch signal tail is longer than that, the intensity measurement could therefore be influenced.

Bunch length σ_t

The bunch length is defined as the standard deviation of the charge distribution (see Section 4.2.1). Because the bunch pulse is highly related with the derivative of this distribution, the time difference between the peak and the valley of the bunch signal is used as a measure of the bunch length (see Figure 5.2d).

Instead of just taking the minimum and maximum sample points, the locations of the peak and valley are found by fitting a quadratic curve to the sample points around the sampled extreme points. The location of the extreme points of these second order polynomials are then calculated. This calculation also gives a continuous distribution of measured bunch lengths.
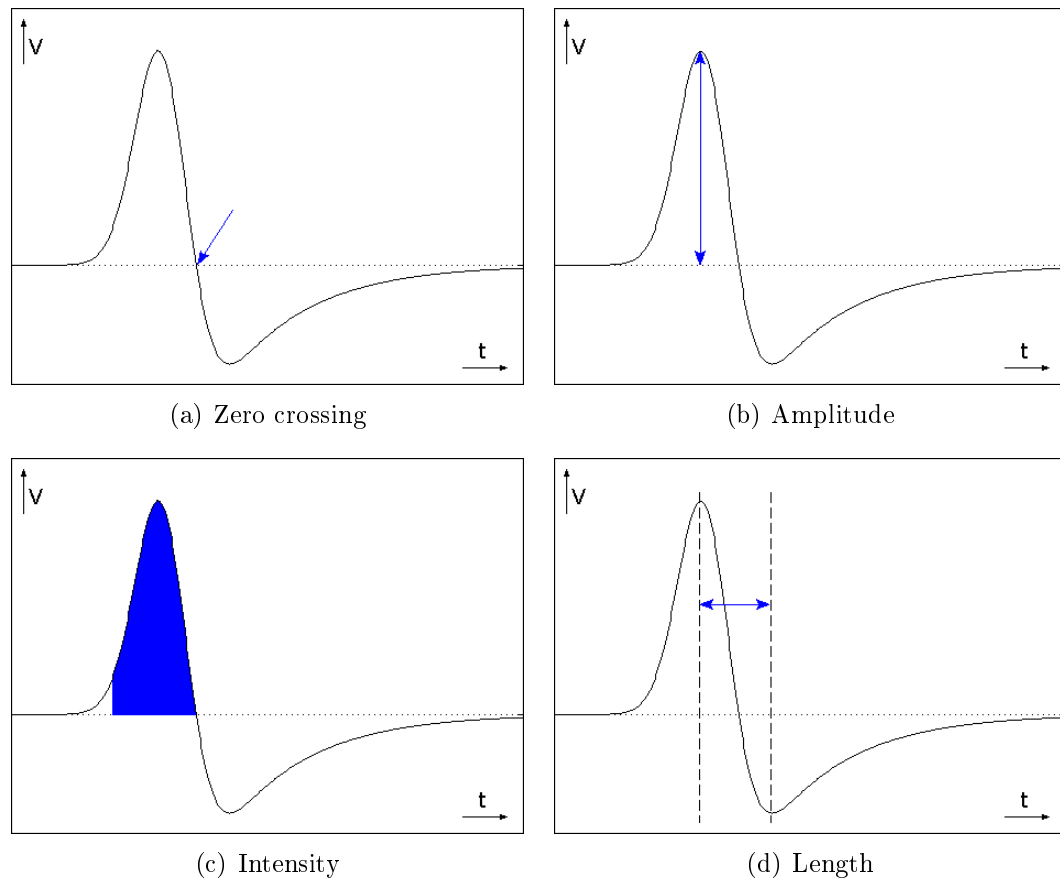

(a) Zero crossing

(b) Amplitude

(c) Intensity

(d) Length

Figure 5.2: Measured bunch parameters.

5.5.2   Square pulse signal processor

To determine the correct timing of the clock and orbit signals, the square pulse signal processor finds all rising and falling edges in these square pulse trains. After a certain threshold is crossed, a window is cut out around the first sample point over the threshold and a polynomial fit is performed. Since it is a continuous function, this fit identifies the threshold crossing much more precisely.

5.6   Phase & BCID associator

After the bunch and square pulse signal processors have analysed the signal waveforms, the Phase & BCID associator will combine the extracted parameters in the BTDs and SPTDs. By relating the location of the bunches from the BTDs with the timing information of the clock edges saved in the SPTDs, the bunches can be assigned a phase. The orbit signal is to be used as a timing reference to identify the bunches in the bunch train. Starting with the first bunch crossing after the orbit tick, the bunch crossings are the tagged in ascending order with the so-called *Bunch Crossing Identifier* (BCID).

 If the orbit pulse is missing for any reason, a reference bunch pattern can be used to give the bunches the correct BCID. The actual series of filled and empty bunch crossings in the bunch signal will be compared with the expected one given in the reference and the goodness of match will be computed. By moving the patterns against each other, the best matching position is then found and will give the BCID offset.

5.7   Storage

The data produced by the monitoring system has to be stored for further on- and offline analysis such as comparisons, trend monitoring, etc. Basic programmes and functions are desired for saving and reading waveforms. The binary format was chosen to save the waveforms in an efficient way. The compressed data in the waveform descriptors allows for saving them in a more readable text format.

 Waveform and waveform descriptor files are planned to be saved in an easily accessible database.

5.8   Display

Depending on the data detail, the beam monitoring system will be able to store up to 30 MB per analysis iteration. This rather big information outcome must be displayed in an understandable way. The following list introduces the various tools which help presenting the information:

- Outlier finder: The outlier finder offers a list of abnormal bunches which differ significantly from the average bunch. The range of acceptance for a parameter

is selected by the user in terms of standard deviations, with a possibility to choose different cut-off values for different parameters.

- Waveform plots: Seeing the actual waveforms becomes important, when studying abnormal bunches. Therefore, a zoom was developed, which makes the interesting parts of an entire LHC bunch train visible after choosing a bunch from a list of e.g. outlying bunches.

- Histograms: A flexible module for customising histograms of values in an array was designed to provide for a quick display of the distribution for any parameter. The standard deviations of values to be included and number of bins can be configured.

- Parameter-over-BCID plots: An easy way to see the development of the various parameters in the beam structure is achieved by simply plotting the values of a parameter against the BCIDs of the corresponding bunches.

5.9 Configuration

The best possible measurement resolution is realised by setting the vertical scale of the oscilloscope according to the expected signal amplitude. The numerous different LHC operation modes will cause the BPTX signal amplitude to vary (as described Section 4.4). Therefore, a programme must be designed, which is able to set the oscilloscope according to the information about the beam coming from the machine. This will be done via DIP.

Furthermore, the software requires some setting to be configured by the user to ensure a correct signal analysis. After being set via a user interface, these settings will be saved in a readable text format.

Chapter 6

Results and discussion

The contents of this chapter were already presented in two CMS Internal Notes (see [20] and [21]).

6.1 Hardware tests

6.1.1 Background

Calculations indicate that an oscilloscope with a bandwidth of at least 500 MHz and a sampling rate of 5 to 10 GS/s, i.e. a time resolution of 100 to 200 ps, is needed (see Chapter 4). In order to capture a full LHC turn it also needs a memory depth of at least 100 μs per channel.

Various scopes fulfil these specifications. The LeCroy WP7100A (see [22]) and WR204Xi (see [23]) and the Tektronix DPO4104 (see [24]), DPO7054 and DPO7104 (see [25]) were borrowed for evaluation. The most interesting model in the WaveRunner Xi series is the 600 MHz version, WR64Xi, but it was not available for evaluation. According to LeCroy, the only difference between the two models is the bandwidth which means they are equivalent in the features tested in this document.

6.1.2 Purpose

The focus of these tests was on scope-computer communication and software stability. A lot of time was also spent investigating the built-in scope software and possibilities for using it for monitoring purposes. The benefit of using these "online" measurements would be to quickly issue an alarm if something goes wrong (e.g. if the BPTX signals and clock signal have different frequencies or if a phase shift occurs between BPTX and clock signal).

6.1.3 Setup

A setup in the ATLAS trigger electronics lab, using custom ATLAS electronics boards and NIM logic modules, allowed producing signals similar to the LHC's BPTX1 and BPTX2 and the RF2TTC outputs *BCmain* and *Orbmain*. The signals were generated in the following way (see Figure 6.1):
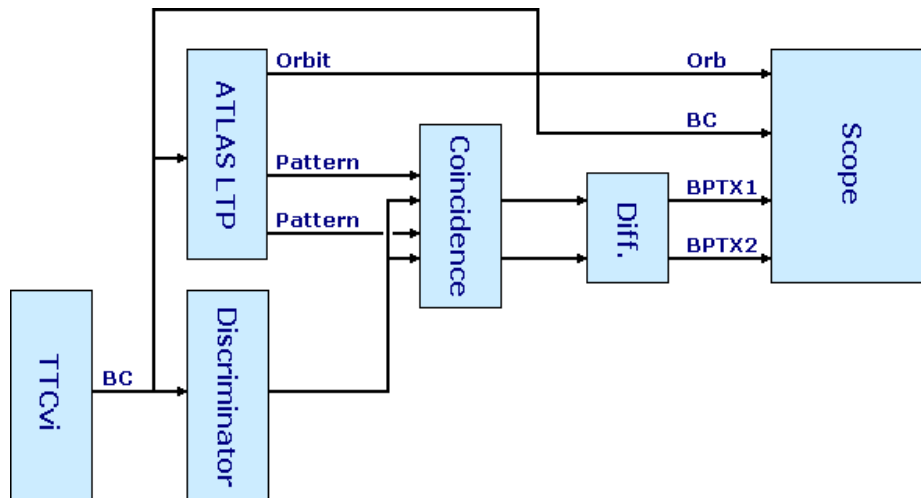
Figure 6.1: The setup in the ATLAS trigger electronics lab.

- Bunch Clock (BC): taken from a TTCvi module (see [26]).

- Orbit signal: Taken from an ATLAS Local Trigger Processor (LTP) (see [27]).

- BPTX1 and BPTX2:

  1. An ATLAS LTP was programmed to generate a pattern of 25 ns pulses corresponding to a full LHC turn with 2808 filled bunches (i.e. 89 μs) (see Figure 6.2a).

  2. The Bunch Clock was used as input to a discriminator to transform it into a "spiky" clock ($\sim$4 ns pulses) (see Figure 6.2b and c).

  3. A coincidence module was used to turn the spiky clock and the bunch pattern pulse train into a bunch train of short pulses (see Figure 6.2d).

  4. A capacitance mounted on the oscilloscope input differentiated the signal to give it characteristics similar to the bipolar pulses expected from the BPTX detectors (see Figure 6.2e).

In Figure 6.3 a photo of the setup in the lab is shown.

6.1.4 Specifications of the tested oscilloscopes

Table 6.1 compares the key properties and specifications for the oscilloscopes considered in these tests (see Figure 6.4a-d).

6.1.5 Specifications of test computers

This list shows the computers used for testing the oscilloscopes. Note that not only different CPUs and network cards, but also different operating systems were used:

- Laptop: Intel Pentium 4, Mobile CPU 1.7GHz, 512MB RAM, OS: WinXP, 10/100 Base-T Ethernet.
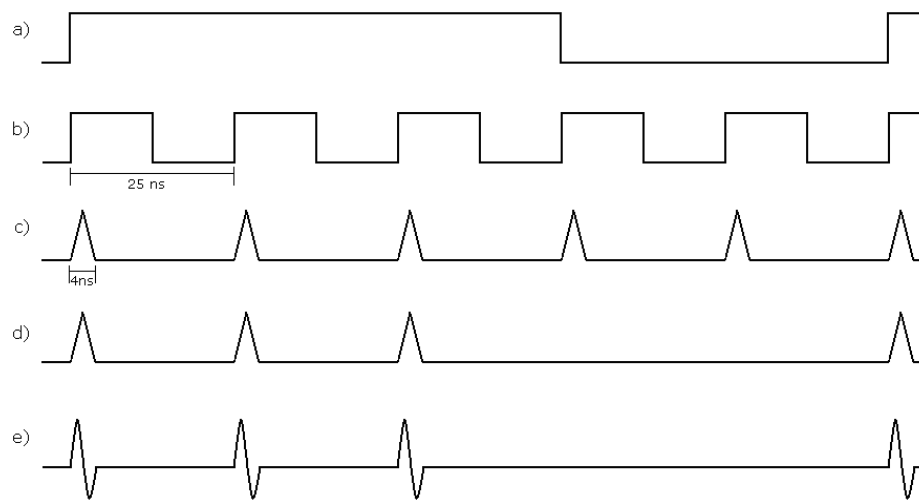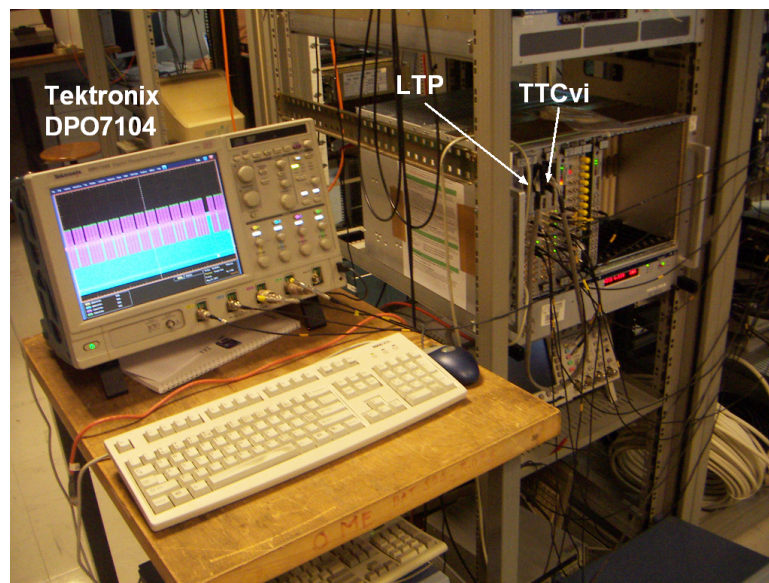
Figure 6.2: Generating the BPTX signals.

Figure 6.3: Photo of the test setup taken in the ATLAS trigger electronics lab. The TTC-VMEbus interface (TTCvi) module interfaces the TTC system to the Central Trigger Processor (Global Trigger).

- PC: Intel Pentium 3, 2x800MHz, 1GB RAM, OS: Linux (SLC 4.3), 10/100 Base-T Ethernet (3Com Corporation 3c905B Deluxe Etherlink 10/100/BNC).

- Rack-PC: Dell PowerEdge 2950, Intel Xeon CPU 2GHz, 3.25GB RAM, OS: WinXP, 10/100/1000 Base-T Ethernet. This is the computer used for the final beam monitoring system at IP5.

For data acquisition, an application was developed in NI LabVIEW and used in all three cases. This software uses oscilloscope-specific drivers to communicate with the hardware. Since LeCroy do not support Linux officially, a special set of drivers was

Table 6.1: Key properties of the tested oscilloscopes.

	LeCroy WP7100A	LeCroy WR64Xi/ WR204Xi	Tektronix DPO7054/ DPO7104	Tektronix DPO4104
Bandwidth (GHz)	1	0.6/2	0.5/1	1
Sampling rate (for 4 channels) (GS/s)	10	5	5 (10 with option 2SR)	5
Memory depth (MPoints)	10	12.5	10	10
LabVIEW drivers	Windows: Yes Linux: Yes	Windows: Yes Linux: Yes	Windows: Yes Linux: Yes	Windows: Yes Linux: Yes
LAN connectivity	10/100 Base-T Ethernet	10/100/1000 Base-T Ethernet	10/100/1000 Base-T Ethernet	10/100 Base-T Ethernet
Dimensions (H/W/D) (mm)	264/397/491	260/340/152	292/451/265	229/439/137
Weight (kg)	18	7	15	5
CPU	Intel Pentium 4, 2.8 GHz processor	Genuine Intel Processor, 1.3 GHz processor	Intel Pentium 4, 3.4 GHz processor (+ 1 processor per channel)	n.a.
PC System Memory (MB)	1000	480	2000	n.a.
Hard Disk Drive (GB)	40	34	80	n.a.
Approx. price (CHF)	25.6k	16.9k (for WR64Xi)	26k/33k	21k
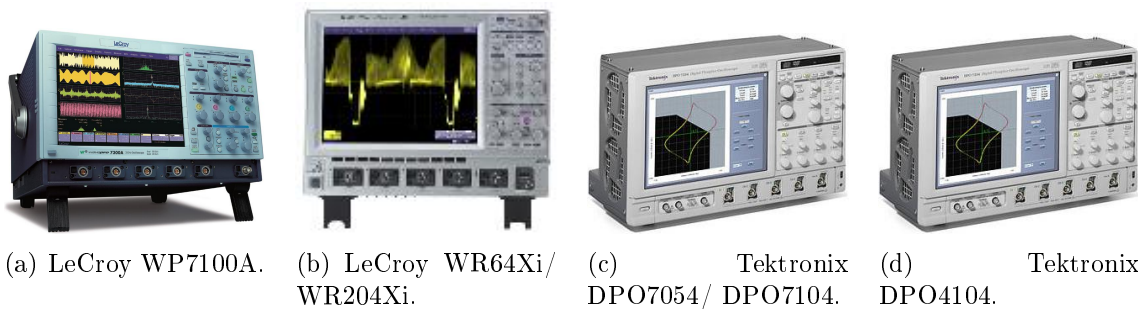
(a) LeCroy WP7100A.   (b) LeCroy WR64Xi/ WR204Xi.   (c)   Tektronix DPO7054/ DPO7104.   (d)   Tektronix DPO4104.

Figure 6.4: Tested oscilloscopes.

developed in order to test their scopes with this platform (see [28]). However, all scopes can be run using either Linux or WinXP.

For most setups the scopes were merely used for acquiring the data and then passing it on the PC for processing (see Figure 6.5a). But since almost all of them had the measurement software running on a WinXP based system (see Table 6.1), they were also tested as a stand-alone measurement device. Therefore, in setups 4, 5, 9 and 10 (see Table 6.2), the analysis software run on the oscilloscopes and no separate computer was used (see Figure 6.5b). For setups 4 and 9, this was done still using the LabVIEW platform, for setups 5 and 10 the programme was compiled and the scope used as a stand-alone measurement device.
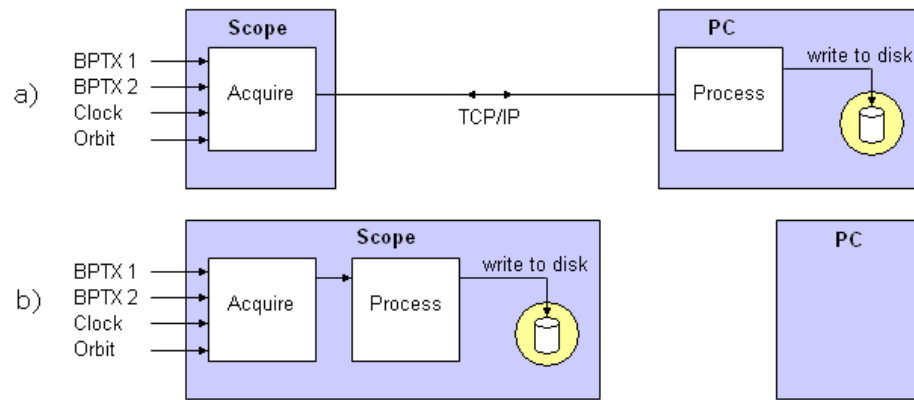
Figure 6.5: Comparing two setup possibilities: scope solely used for DAQ (a) and also for processing and storing data (b).

6.1.6 Test description

The test program was designed to test the stability of the computer-scope connection and the robustness of the analysis software. In addition, the iterative nature of the test program allowed us to study the time needed for both data acquisition and each step of the analysis. Consequentially, the steps were therefore performed in sequence and time stamps were taken between each step. In the final program several steps could be completed simultaneously, resulting in an even higher monitoring frequency. The steps performed in each iteration are described in the following sections (compare with Chapter 5).

Acquisition and data transfer

A command is sent to the oscilloscope telling it to send the data stored in memory. The data is then transferred to the computer running the analysis software via TCP/IP. This was true for all the setups except 4 and 5 where the software running on the Tektronix DPO7104 scope thinks that it is communicating via GPIB. The measured period for all tests was 100 μs.

Waveform processing

Each of the captured waveforms is processed sample by sample to extract the interesting information. This first step of the analysis returns a description of the identified bunches in a more condensed data structure. There are four signals to be processed - BPTX1, BPTX2, clock and orbit. In the BPTX bunch train, the individual bunches can be described by the time of arrival, amplitude, intensity and length.

Associating phase and assigning Bunch Crossing Identifier

By combining the bunch timing information with the location of the edges of the clock signal, bunches can be assigned to a phase. The orbit signal is used as a time

reference to determine the bunch location in the bunch train. The bunch crossings are numbered sequentially starting with the first bunch crossing after the orbit pulse. This number is called Bunch Crossing Identifier (BCID).

6.1.7 Results

In general, the tests showed that the connection between the oscilloscopes and the computers is stable. In total, several hundreds of thousand iterations were completed without a single communication breakdown. The results from the different setups used for long term run tests are listed in Table 6.2. The average time needed to complete each step of the program is presented along with their corresponding standard deviation. In addition, the column Runs contains the number of completed runs for each hardware configuration.

Table 6.2: Various setups and times for long term run tests. In the column software (SW) type, ".vi" means the software was run using LabVIEW and ".exe" means it was run with a compiled, executable programme. The time values are given in means and standard deviations.

Test #	Scope	Platform/system	SW type	Runs	Acquisition time (s)	BPTX1 processing time (s)	BPTX2 processing time (s)
1	Tektronix	WinXP/Laptop	.vi	58978	1.29 ± 0.06	0.18 ± 0.03	0.18 ± 0.02
2	DPO7104	Linux/PC	.vi	24344	3.06 ± 0.05	0.63 ± 0.06	0.59 ± 0.05
3		WinXP/Rack-PC	.vi	2906	0.65 ± 0.09	0.06 ± 0.01	0.06 ± 0.01
4		WinXP/on-scope	.vi	29168	1.23 ± 0.06	0.08 ± 0.00	0.08 ± 0.00
5		WinXP/on-scope	.exe	23675	1.23 ± 0.07	0.06 ± 0.01	0.03 ± 0.00
6	LeCroy	WinXP/Laptop	.vi	64402	1.45 ± 0.15	0.17 ± 0.02	0.10 ± 0.01
7	WP7100A	Linux/PC	.vi	36271	4.86 ± 0.16	0.39 ± 0.01	0.39 ± 0.01
8		WinXP/Rack-PC	.vi	2011	1.10 ± 0.13	0.08 ± 0.01	0.07 ± 0.01
9		WinXP/on-scope	.vi	17333	1.96 ± 0.30	0.09 ± 0.01	0.06 ± 0.01
10		WinXP/on-scope	.exe	75620	1.92 ± 0.38	0.08 ± 0.01	0.05 ± 0.00
11	Tektronix	Linux/PC	.vi	3781	5.73 ± 0.10	0.52 ± 0.03	0.52 ± 0.01
12	DPO4104	WinXP/Laptop	.vi	4971	4.72 ± 0.06	0.23 ± 0.04	0.21 ± 0.03
13	LeCroy WR204Xi	WinXP/Rack-PC	.vi	42899	0.34 ± 0.07	0.04 ± 0.01	0.04 ± 0.01

Test #	Orbit processing time (s)	Clock processing time (s)	BCID and phase association time 1 time (s)	BCID and phase association time 2 time (s)	Total time (s)
1	0.07 ± 0.01	1.28 ± 0.08	0.52 ± 0.03	0.53 ± 0.04	4.06 ± 0.19
2	0.31 ± 0.01	2.78 ± 0.08	1.33 ± 0.09	1.37 ± 0.02	10.07 ± 0.20
3	0.02 ± 0.01	0.52 ± 0.01	0.27 ± 0.01	0.27 ± 0.01	1.83 ± 0.09
4	0.03 ± 0.00	0.63 ± 0.01	0.27 ± 0.00	0.27 ± 0.00	2.58 ± 0.06
5	0.03 ± 0.00	0.57 ± 0.01	0.06 ± 0.01	0.21 ± 0.01	2.21 ± 0.07
6	0.08 ± 0.01	1.26 ± 0.08	0.51 ± 0.03	0.50 ± 0.02	3.63 ± 0.21
7	0.33 ± 0.01	2.92 ± 0.30	1.31 ± 0.01	1.32 ± 0.01	11.52 ± 0.35
8	0.01 ± 0.01	0.53 ± 0.01	0.34 ± 0.01	0.35 ± 0.01	2.48 ± 0.14
9	0.04 ± 0.04	0.77 ± 0.02	0.30 ± 0.01	0.08 ± 0.02	3.31 ± 0.30
10	0.04 ± 0.01	0.75 ± 0.02	0.24 ± 0.01	0.04 ± 0.01	3.11 ± 0.38
11	0.34 ± 0.01	4.87 ± 0.18	3.00 ± 0.01	3.01 ± 0.01	17.97 ± 0.22
12	0.07 ± 0.01	2.28 ± 0.12	1.50 ± 0.07	1.50 ± 0.08	10.52 ± 0.26
13	0.01 ± 0.01	0.45 ± 0.01	0.27 ± 0.01	0.26 ± 0.02	1.41 ± 0.08

In Figure 6.6, Figure 6.7 and Figure 6.8, the results for different scopes using the same computer are compared. The dark blue bars represent the data acquisition

and transfer time, all other bars represent the different parts of the analysis time. It can be seen, that depending on the setup one gets between 6 and 40 acquisitions per minute.
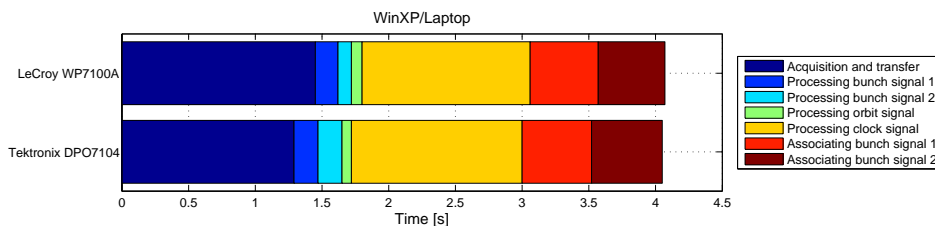

Figure 6.6: Process times for setups 1 and 6 given in Table 6.2.
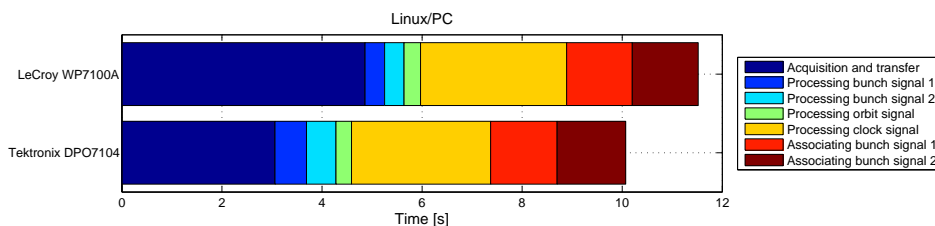

Figure 6.7: Process times for setups 2 and 7 given in Table 6.2.

The setups with the Linux-PC are by far the slowest and the most likely reason for this is the inferior hardware of this computer.
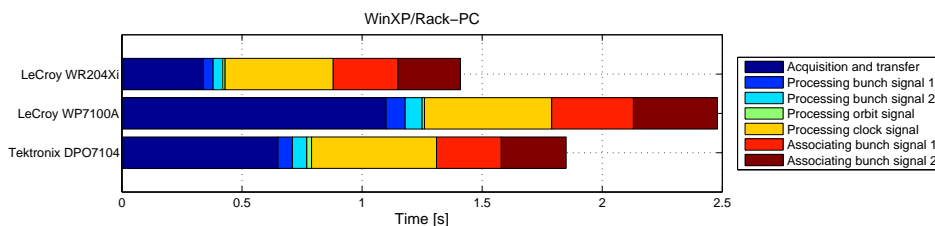

Figure 6.8: Process times for setups 3, 8 and 13 given in Table 6.2.

As it can be seen in Figure 6.8, the fastest configuration was the LeCroy WR204Xi with the Rack-PC running WinXP (setup 13). Compared with results from the Tektronix DPO7104 using the same PC (setup 3), there are hardly any differences in the various processing times. The major difference is in the acquisition time, which is 0.34 ± 0.07 s for the WR204Xi and 0.65 ± 0.09 s for the DPO7104. The reason for this is that only half the amount of data is transferred since the sampling rate for the LeCroy model is only 5 GS/s for this scope. With this in mind, the WR204Xi is comparable to the DPO7104, since they are both equipped with 10/100/1000 Base-T Ethernet.

To check, how the acquisition time changes with increasing record length, 100 iterations per record length were done using the setups 1, 6 and 12. In general, oscilloscopes acquire data only in fixed record lengths, given in data points:

- DPO7104: 1k, 5k, 10k, 20k, 50k, 100k, 200k, 500k, 1M, 2M, (5M and 10M)

- WP7100A: 1k, 2.5k, 5k, 10k, 25k, 50k, 100k, 250k, 500k, 1M, 2.5M, (5M and 10M)

- DPO4104: 1k, 10k, 100k, 1M (and 10M)

Values above 1MPoints, 2MPoints and 2.5MPoints respectively could not be tested since the laptop running WinXP was not able to process the amount of data anymore. Figure 6.9 shows how the acquisition and transfer time changes over increasing record length. The unusually large error bar on the last point of the LeCroy WP7100A series is also due to the limits in hardware performance.
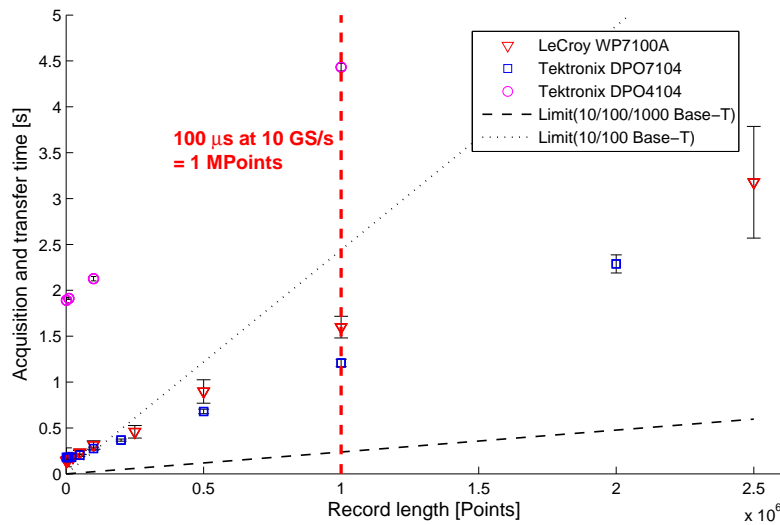
Figure 6.9: Change of acquisition and transfer time over size of data using setups 1, 6 and 12 respectively and 100 iterations per record length. Error bars represent the standard deviation.

LabVIEW converts the data into an array of doubles, which means 8 bytes per point and channel. Therefore, a record length of 1 MPoints for 4 channels corresponds to about 30 MB of data. This would mean a transfer time of 0.24 s for a 10/100/1000 Base-T connection and 2.44 s for 10/100 Base-T (see Figure 6.9 for the limits for the two types of Ethernet cards). Setups 1, 6 and 12 were done with the WinXP laptop, which only has a 10/100 Base-T card. So, it can be seen clearly that the scopes send their data in some compressed way.

6.1.8 Built-in software evaluation

Both of the scopes have built-in functions for measuring quantities like phase, frequency, period times, etc. However, these measurements could not be easily applied to our special scenario (e.g. because of gaps in the BPTX signals etc.). Even after discussing with application engineers at LeCroy and Tektronix, not even a simple

histogram of the phases of each bunch and its closest clock edge could be created. Looking for deviations and irregularities on the BPTX signal was also not possible.

The idea of using the scopes' memory segmenting features (e.g. "FastFraming") for performing measurements on individual bunches also failed since there was no way to get hold of the individual measurements (nor keeping track of which value belongs to what bunch). For all models, the task to simply make frames of 25 ns around every bunch, perform some measurement (e.g. maximum amplitude or zero crossing) and save with a timestamp, failed. First of all, the deadtime between the frames made it impossible to retrieve individual bunch information for an entire bunch train and when data is stored, there was no relation between the data and the time it was stored.

6.1.9 Additional remarks

Several other properties and features of the various scopes are shown in Table 6.3.

Table 6.3: Additional features and properties of the considered scopes.

	LeCroy WP7100A	LeCroy WR64Xi/ WR204Xi	Tektronix DPO7054/ DPO7104	Tektronix DPO4104
Remote reboot	Boots when re-powered. Can therefore be rebooted in case of hanging system by remotely turning the crate power off and on.	Boots when re-powered. Can therefore be rebooted in case of hanging system by remotely turning the crate power off and on.	Can be booted remotely when shut down by "Wake on LAN". Internal VXI-11 LAN-Server has to be set to default ON in BIOS.	Boots when re-powered. Can therefore be rebooted in case of hanging system by remotely turning the crate power off and on.
External Trigger	Has all trigger options as a regular channel	Has all trigger options as a regular channel	Has all trigger options as a regular channel	Has all trigger options as a regular channel
AB-Trigger	Can only trigger on edges, levels and patterns for the B event	A: edge, state, pattern, pat-state, B: edge, width, glitch, interval	Has all trigger options for the B event	Can only trigger on edges and levels for the B event
Maximum input voltage	5 V_{RMS}, changes automatically to GND for higher peaks	5 V_{RMS}	5 V_{RMS} with peaks $\leq \pm 24\text{V}$	5 V_{RMS} with peaks $\leq \pm 20\text{V}$
Masks	Masks are learned from signals, but do not change with range or time offset.	Masks are learned from signals, but do not change with range or time offset.	Masks have to be typed in by hand.	n.a.
Replacement policy	Replacement scope within 1-2 days; scope maintenance guaranteed for 7 years minimum; repair time 8 days		No guaranteed replacement device; warranty possible for 10 years (R10 contract); repair time 12-21 days	
	Neither of the manufacturers had a real replacement policy. What is stated here was promised by the company representatives via email.			

In general, after an initial learning period, all scopes were more or less easy to handle. The control via touch screen was difficult at the beginning, but it turned to be actually very handy. The LeCroy WP7100A and the Tektronix DPO7054 (and DPO7104 respectively) had both a very good display, although with 12.1" the Tektronix model was bigger compared to LeCroy's 10.4". The all-over smaller size of the LeCroy WR64Xi (and WR204Xi respectively) results in only one set of buttons

for all four channels but it still has the 10.4" display. However, the reduction in weight and size made it very handy.

6.1.10   Conclusions

The LeCroy WR204Xi is by far the fastest when it comes to data acquisition. Since a scope bandwidth of 2 GHz is not needed (see section 6.1.1), the LeCroy WR64Xi is recommended for the BPTX read-out. It fulfils the requirements the best and is also the cheapest. The 600 MHz bandwidth is enough when considering that most of the higher frequencies are already heavily attenuated by the transmission line. A sampling rate of 5 GS/s would give about 30 samples on a bipolar BPTX pulse caused by a nominal LHC bunch and about 6-7 data points between its peak and valley (see Figure 6.10).
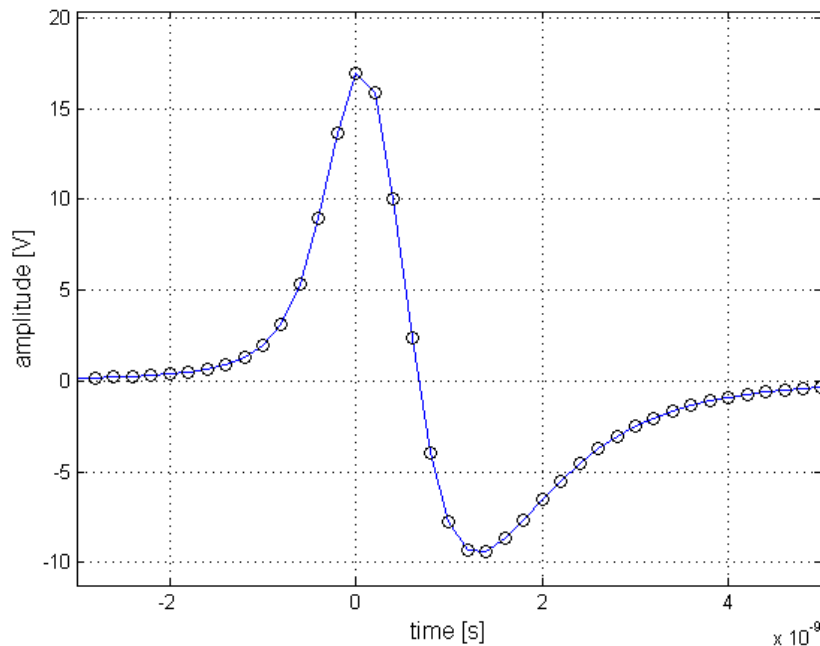
Figure 6.10: Expected BPTX signal for nominal LHC intensity sampled with 5 GS/s.

Although these tests focused on the oscilloscopes, the results also show what is required for the computer that runs the analysis in order to achieve good performance. A well-equipped modern PC should do the job well as long as it is equipped with at least one gigabyte (preferably two) of memory. Most importantly it needs to have dual network cards that support Gigabit Ethernet to enable quick data transfer, both to and from the oscilloscope and the network.

6.2 SPS measurements

6.2.1 Background

On June 13th - 15th, 2007 measurements were done on a real BPTX signal from a BPTX station at the SPS (Bat. 921, BA4) together with Christian Ohm (for ATLAS BPTX). Since the same type of pick-up and cable is installed at the SPS and the LHC, the measurements here allow verifying the signal shape and also test the system in real conditions. Measurements were made with the LeCroy WR204Xi (see [23]) and the Tektronix DPO7054 (see [25]) to compare their performance, following up on tests carried out earlier this year in the ATLAS trigger electronics lab.
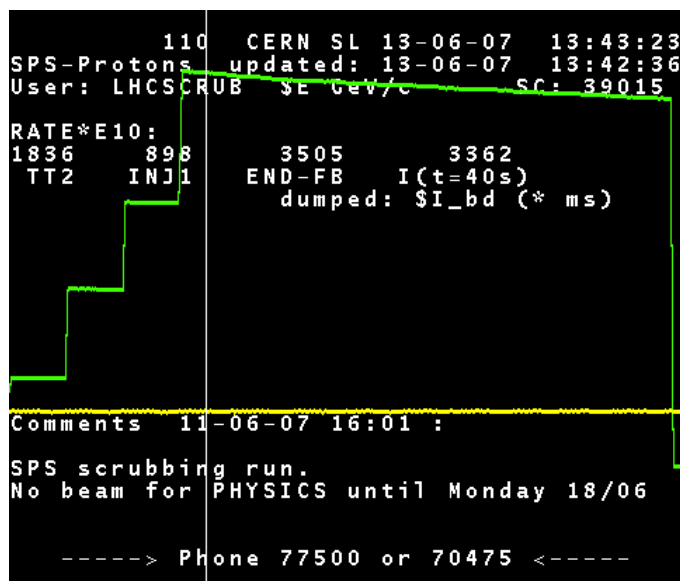
Figure 6.11: Status screen at the SPS during the test beam.

During these beam tests, the SPS accelerator was filled and emptied repeatedly. Figure 6.11 shows the beam intensity (green curve) over time for an SPS cycle. On both days the SPS was in "scrubbing run" coasting at 26 GeV (i.e. no ramp), with one cycle lasting 43.2 s. The number of batches per fill varied from 1 to 4, maximized compatibly with the MKE heating (extraction kicker magnets) and the vacuum, keeping the maximum duty factor (see Figure 6.12). The batches contained 72 filled bunches with 25 ns spacing. The number of protons per bunch was $1.3 \cdot 10^{11}$ (see [29]), which is between the LHC nominal ($1.15 \cdot 10^{11}$ ppb) and ultimate intensity ($1.67 \cdot 10^{11}$ ppb).

The cable length from the pick-ups to the control room at the SPS is 150 m (cable type: Nexans CMA 50) and the bunch time standard deviation was 0.75 ns (see [30]), which corresponds to a length of 0.2247 m. With these parameters the expected signal can be calculated. For the calculation, the linear charge distribution along the beam line is approximated by a Gaussian function. From the charge collected on the button, the resulting current can determined. Convoluting this
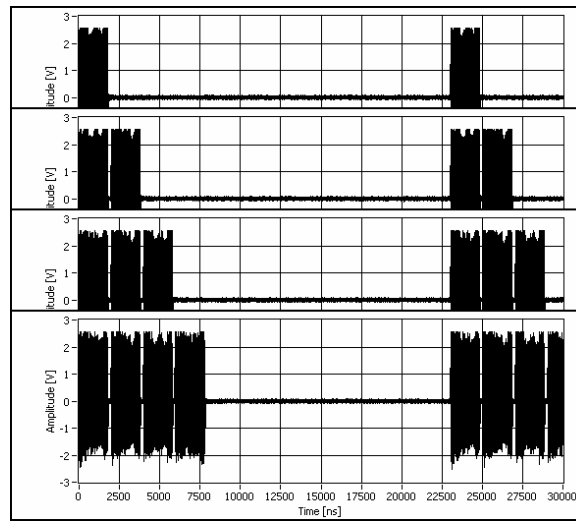
Figure 6.12: Different filling schemes during the SPS scrubbing run as measured by the oscilloscope-based BPTX read-out (see section 6.2.2)

with the button impedance (consisting of cable resistance and button capacitance) results in the voltage which is to be expected (see Chapter 4). Figure 6.13 shows the calculated signal at the pick up electrodes, after the cable and with the effects of a 2-GHz-scope.
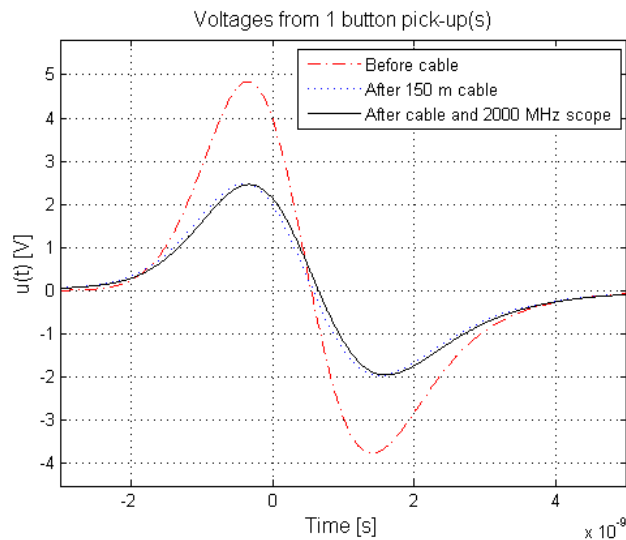

Figure 6.13: The expected signal voltage at the button, after the transmission line and after both transmission line and oscilloscope bandwidth effects (for the WR204Xi) is taken into account.

After taking cable and oscilloscope effects into account, the expected signal maximum for the WR204Xi is 2.38 V, the area under the positive half of the curve is $3.84 \cdot 10^{-9}$ Vs, which corresponds to a charge of $7.69 \cdot 10^{-11}$ C, and its length from peak to valley is predicted to be 1.93 ns.

6.2.2 Setup

The measurements were done with the setup shown in Figure 6.14. Unfortunately only one button electrode was able to be used; the other ones were used for another application at this time. Note that for the ultimate BPTX system used for monitoring the LHC, the signal is a sum of four buttons. The BOBR card supplied a clock and an orbit signal (see [31]). To test the read-out and processing system as it is used for the LHC, the acquisition time was set to 100 μs, thus capturing a little more than 4 SPS orbits (23.1 μs). In Figure 6.12 one can see the first 30 μs for different filling schemes.
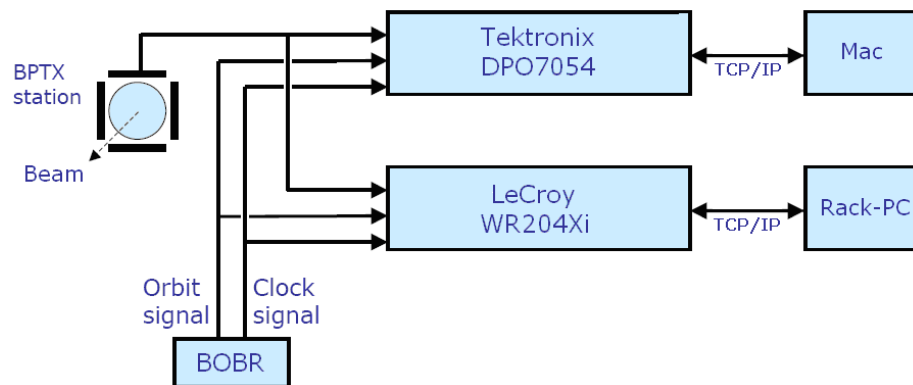
Figure 6.14: Setup for the measurements at the SPS testbeam: the two oscilloscopes were connected to the same button electrode.

Specifications of test computers

This list shows the computers used for testing the oscilloscopes. Note that not only different CPUs, but also different operating systems were used:

- Rack-PC: Dell PowerEdge 2950, Intel Xeon CPU 2GHz, 3.25GB RAM, OS: WinXP, 10/100/1000 Base-T Ethernet

- Mac: Intel Core2 Duo 2GHz CPU, 1GB RAM, OS: OS X 10.4.10 (Tiger), 10/100/1000 Base-T Ethernet

In Figure 6.15 a photo of the setup in the control room is shown.

6.2.3 Acquired signals

BPTX signal

Figure 6.16 shows the expected signal compared with one sampled bipolar pulse from the acquired BPTX signal traces.

Just by visually comparing the acquired with the calculated signal, it can be seen that the model agrees very well with the measurement considering the pulse height. Furthermore, the slope between peak and valley matches the data points, so there is
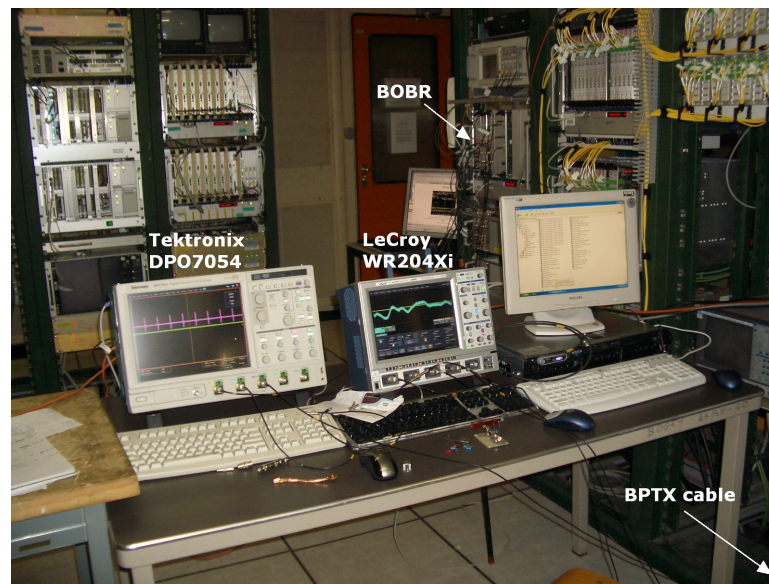
Figure 6.15: Photo of the test setup taken in the SPS control room showing the equipment used.
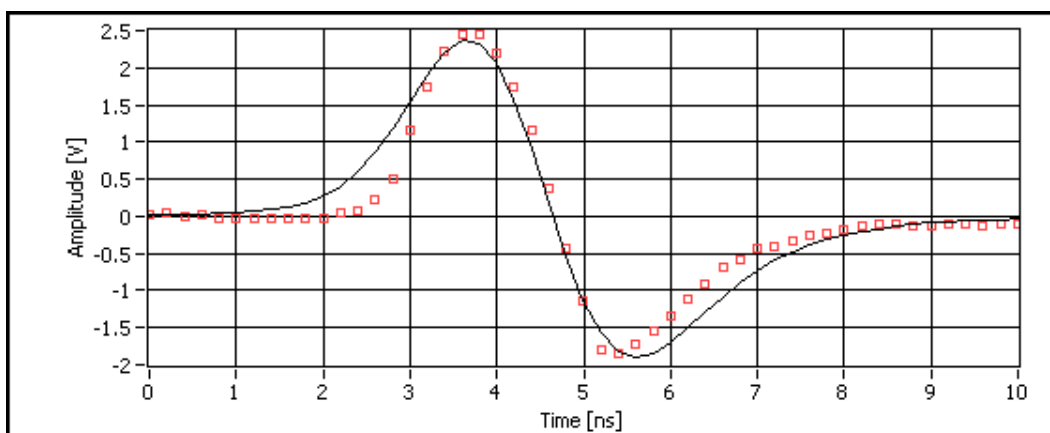
Figure 6.16: Example of a bunch signal from a BPTX signal trace (data points) superimposed with the expected signal (black solid line).

also a very good agreement in the zero crossing. The position of the valley is slightly off, resulting in a small difference in the distance between peak and valley.

The area under the pulse does unfortunately not seem to agree at all. This can be due to the fact, that the model was made for the LHC BPTX button electrodes, so the one installed for the SPS might have a different capacitance. Also the cable length was only estimated to be 150m.

Figure 6.17 shows all bipolar bunch signals of one bunch train superimposed with the expected pulse. A very good agreement with the calculation can be seen. The vertical range has an 8-bit resolution, so for a range of 10.32 V this means 40.3 mV for the least significant bit (lsb).

Since only data is acquired which is displayed on the screen of the oscilloscope,
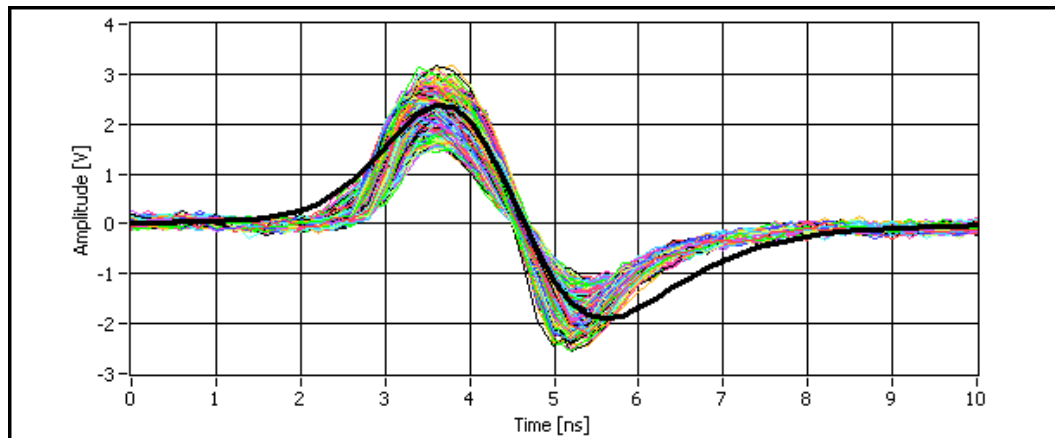
Figure 6.17: 1437 bipolar pulses superimposed with the calculated expected signal (thick black line).

care has to be taken during operation to ensure that the range is always set appropriately for capturing the whole signal but without loosing too much information to digitisation.

Clock signal

The BOBR card provides a 40.08 MHz bunch clock. For the LHC, the clock frequency will also be 40.08 MHz (i.e. 24.95 ns clock period) (see [32]). Figure 6.18, Figure 6.19 and Figure 6.20 show superimpositions of 200 traces of the clock signal coming from the BOBR card. The vertical range was set to 5.16 V, so the lsb for these acquisitions is also 20.2 mV.
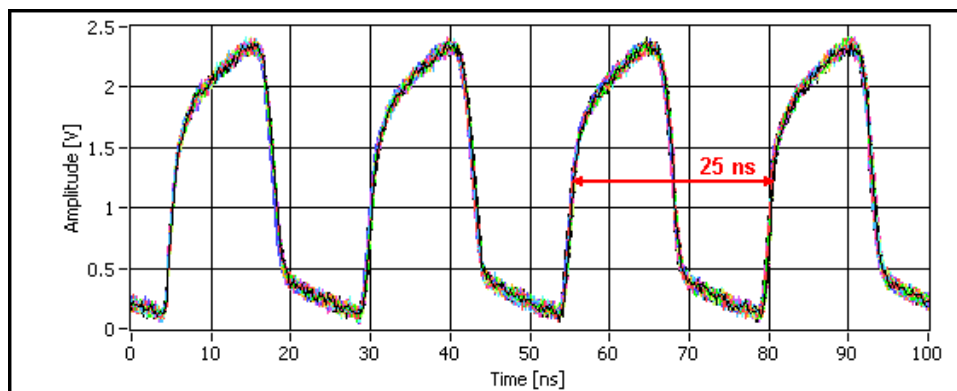
Figure 6.18: Superimposition of clock pulses 1-4 of 200 traces aligned at the 1V-threshold-crossing of the first clock pulse.

This shows that not only the timing but also the pulse height of the signal coming from the BOBR card is very stable, since there is a spread in the amplitude of only about 5%.

Here one can see by eye, that the spread is about what the time resolution of the oscilloscope allows, namely around 200 ps.
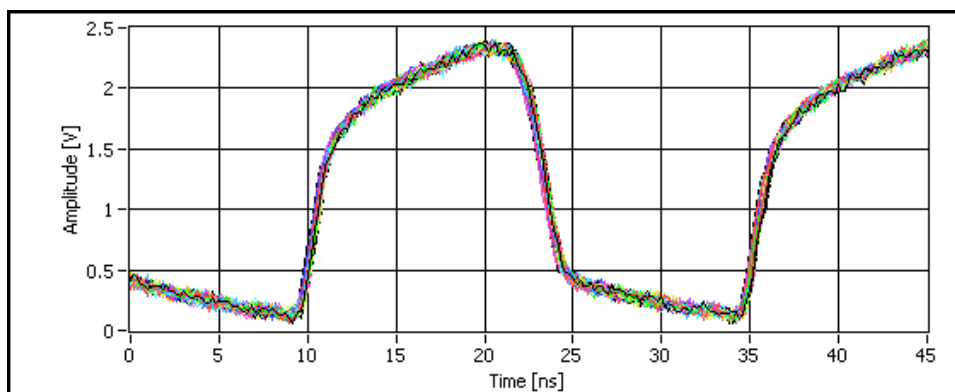
Figure 6.19: Superimposition of the third clock pulses of 200 traces.
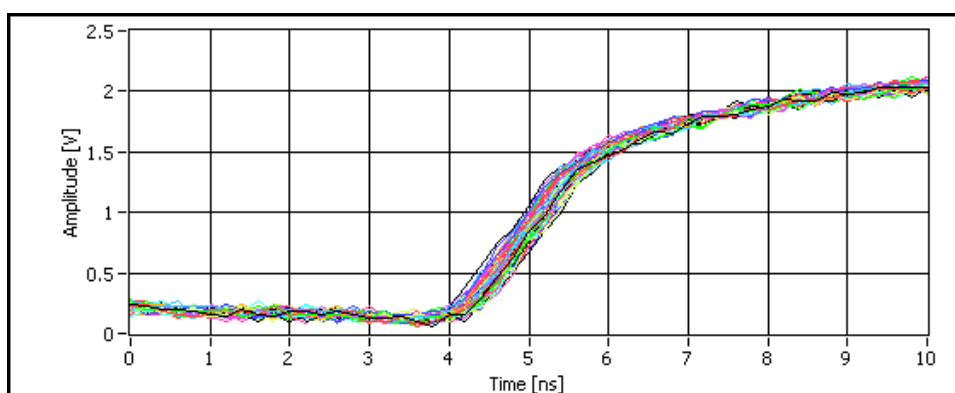
Figure 6.20: Superimposition of the positive edges of the third clock pulses of 200 traces.

Orbit signal

The BOBR card supplies the local turn clock, corresponding to the orbit frequency. This locked either at $1/924$ of the bunch frequency for SPS or $1/3564$ of the bunch frequency for LHC. Thus, for the LHC, the orbit frequency will be 11.246 kHz (i.e. 88.9 μs orbit period) (see [11]). Figure 6.21 and Figure 6.22 show superimpositions of 200 traces of the orbit signal provided by the BOBR card. Again the vertical acquisition range was set to 5.16 V.

The spread in signal amplitude for the orbit signal is also about 5%.

6.2.4 Measurements

The test program was only a slightly modified version from the performance tests done earlier this year in the ATLAS trigger electronics lab (see Section 6.1). The steps performed in each iteration are described in the following sections (compare with Chapter 5).
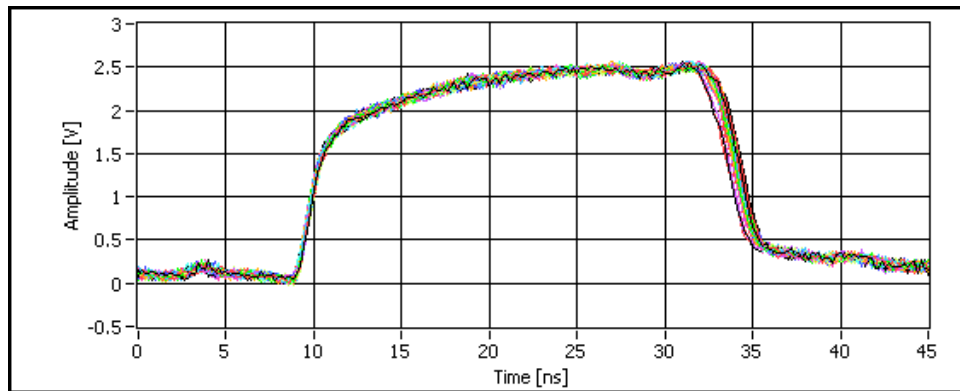
Figure 6.21: Superimposition of the first orbit pulses of 200 traces aligned at the 0.5V-threshold-crossing of the pulse.
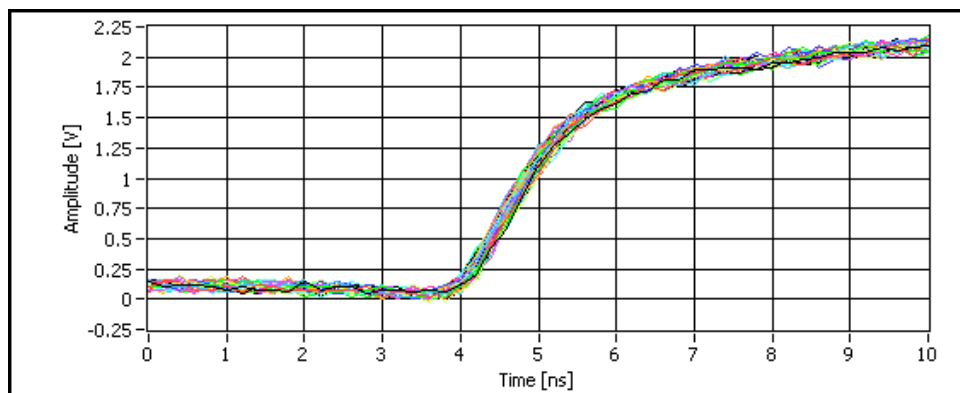
Figure 6.22: Superimposition of the positive edges of the first orbit pulses of 200 traces.

Acquisition and data transfer

A command is sent to the scope telling it to send the data stored in memory. The data is then transferred to the computer running the analysis software via TCP/IP.

Waveform processing

Each of the captured waveforms is traversed sample by sample to extract the interesting information. This first step of the analysis returns a description of the identified bunches in a more condensed data structure. In the case of the SPS test, there were three signals to be processed - BPTX, clock and orbit (since only one button was used). In the BPTX bunch train, the individual bunches can be described by the time of arrival, amplitude, intensity and length.

Associating phase and assigning Bunch Crossing Identifier

The positions of positive and negative clock and orbit edges are determined by fitting a third-order polynomial to the sample points around the edge and calculating the

time when the fit crosses a threshold. By combining the bunch timing information with the location of the edges of the clock signal, bunches can be assigned to a phase. The orbit signal is used as a time reference to determine where bunches are located in the bunch train. The bunch crossings are numbered sequentially starting with the first bunch crossing after the orbit pulse. This number is called Bunch Crossing Identifier (BCID).

6.2.5 Results

The results for center and deviation values of the plots in the following sections are based on the Gaussian fits shown in these plots (black curve). The values given in the histograms are the mean and standard deviation values from the fits. The goodness of fit factor R^2 (also called coefficient of determination), describing how well the fitted model matches the original data set, was computed with NI LabVIEW. This normalized statistical parameter is defined by the following equation:

$$R^2 = 1 - \frac{\sum_{i=0}^{n-1}(y_i - f_i)^2}{\sum_{i=0}^{n-1}(y_i - y)^2} \tag{6.1}$$

where y_i is the ith element of the array of dependent values of the original data set with mean value y and f_i is the ith element of the fitted data array. Thus, the closer the R^2 value is to 1, the better the fit.

Bunch parameters

The results for the bunch parameters amplitude, intensity and length, as described in Section 6.2.4, are shown in Figure 6.23 till Figure 6.25. The blue bars in the plots mark the expectation values.
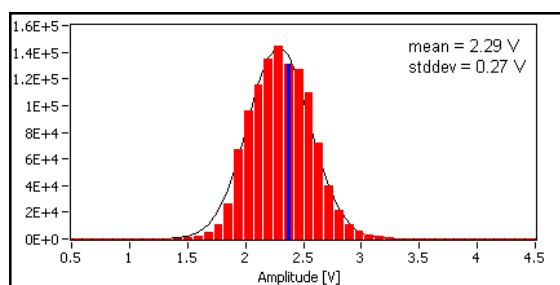
Figure 6.23: Bunch amplitude: R^2 = 0.9905.
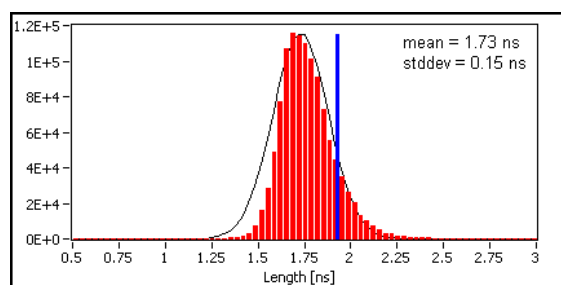
Figure 6.24: Bunch length: R^2 = 0.9470.

The bunch length and amplitude agree rather well with the prediction, considering the SPS cable length was only given approximately. The intensity is lower than the expected value, since the modeled signal has a slower rise then the real one (see Figure 6.16). The charge distribution in Figure 6.26 was calculated by simply dividing the computed bunch intensity given in Vs by 50 Ω, which was the termination of the oscilloscope.
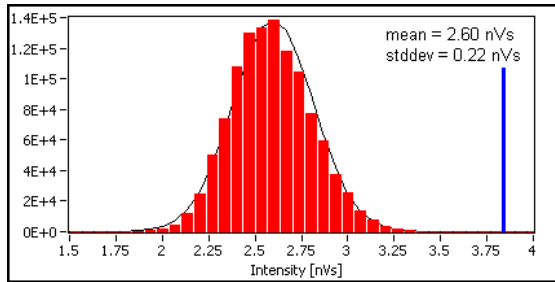
Figure 6.25: Bunch intensity (given in nVs = Nanovolt seconds): R^2 = 0.9884.
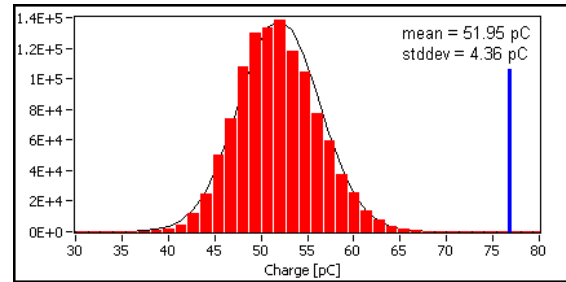

Figure 6.26: Corresponding charge: $R^2 = 0.9884$.

The scatter plots in Figure 6.27 and Figure 6.28 show that the intensity is proportional to the amplitude and inversely proportional to the bunch length. As expected from the model, the bunch amplitude is also inverse proportional to the length (see Figure 6.29).
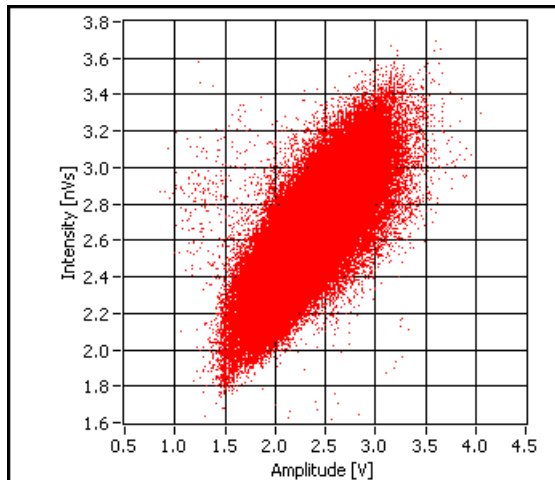
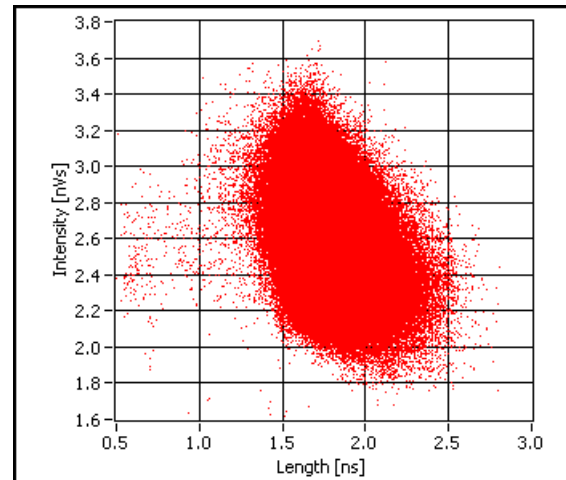

Figure 6.27: Scatter plot: bunch intensity versus amplitude.

Figure 6.28: Scatter plot: bunch intensity versus length.

To check for systematical errors, Figure 6.30 shows the bunch amplitude plotted against the bunch crossing ID number. From this it can be concluded that there is no correlation between the amplitude and its location in the acquired bunch train.

Timing

Figure 6.31 - Figure 6.36 show arrival times of the first bunch crossing, orbit edge and clock with respect to the start of data acquisition and to each other. This was done for 1912 traces. The trigger jitter is given to be ≤ 3 ps rms (see [23]).

This shows that for all signals the timing resolution is at the limit of the oscilloscope, i.e. 200 ps$/\sqrt{3} = 115$ ps.
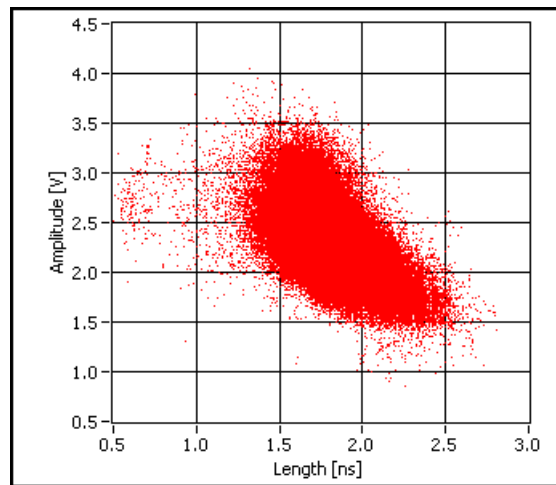
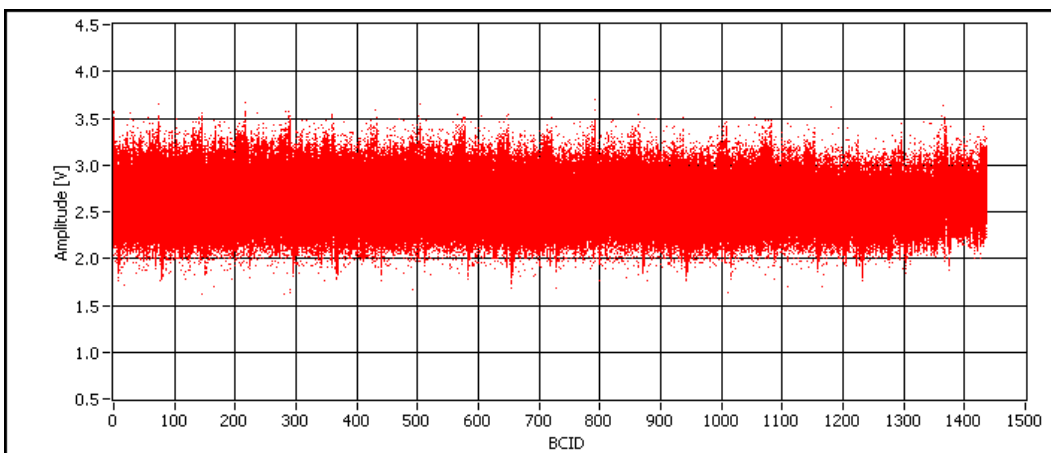**Figure 6.29:** Scatter plot: bunch amplitude versus length.

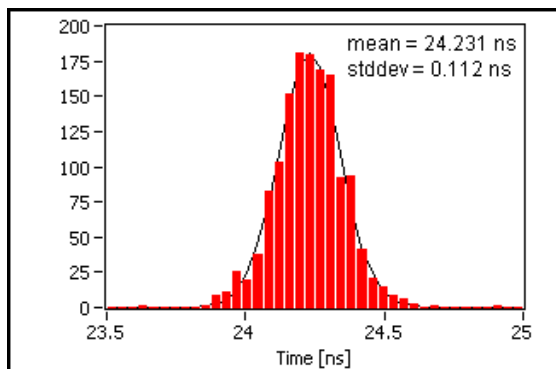**Figure 6.30:** Scatter plot: bunch amplitude versus BCID.

Figure 6.31: Arrival of first bunch zero crossing with respect to start of data acquisition: $R^2 = 0.9866$.
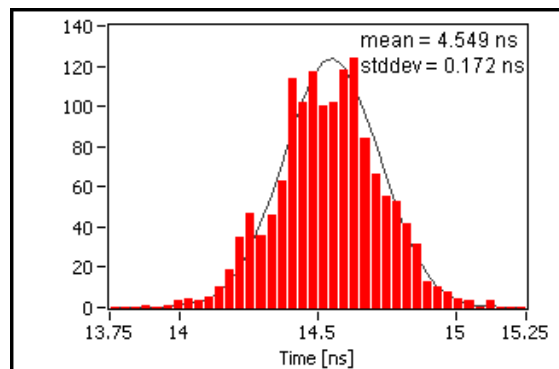
Figure 6.32: Arrival of first clock edge with respect to start of data acquisition: $R^2 = 0.9517$.
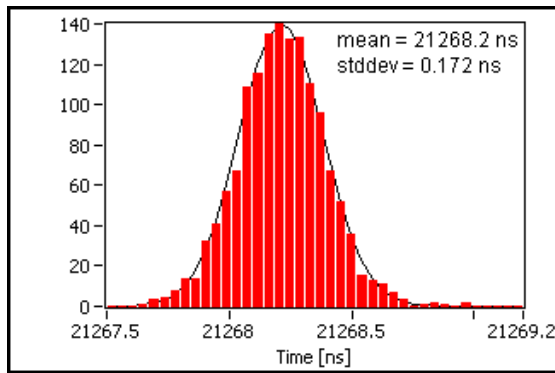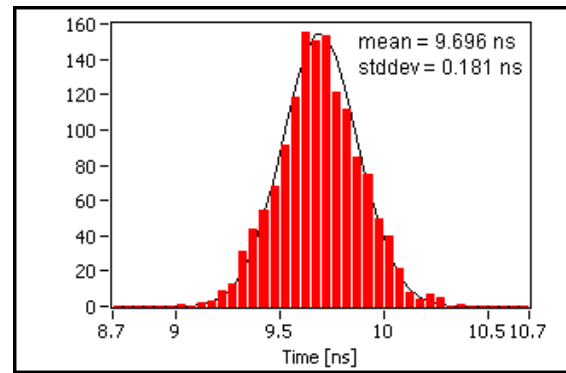
Figure 6.33: Arrival of first orbit edge with respect to start of data acquisition: $R^2 = 0.9942$.

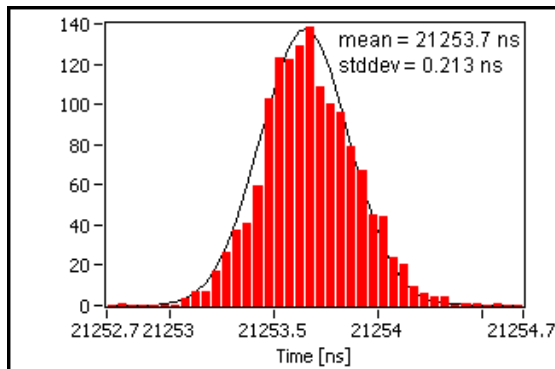**Figure 6.34:** Arrival of first bunch zero crossing with respect to first clock edge: $R^2 = 0.9858$.

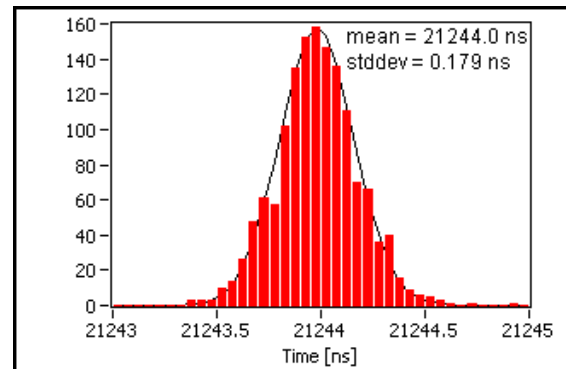**Figure 6.35:** Arrival of first clock edge with respect to first orbit edge: $R^2 = 0.9741$.

Figure 6.36: Arrival of first bunch zero crossing with respect to first orbit edge: $R^2 = 0.9851$.

Timing stability

There are 4005 clock ticks per acquired 100 μs. In order to test the stability of the oscilloscope time base over this whole acquisition time, the arrival time of each positive clock edge with respect to start of data acquisition was determined. Then, standard deviation value (sigma) for these arrival times were computed over 1912 traces. This was done in the same way as for the first positive clock edge (see Figure 6.32).

Figure 6.37 shows the deviation of each clock arrival time plotted against its position in the acquisition.

Figure 6.38 and Figure 6.39 show linear and logarithmic histograms of the deviation of clock arrival time.

Therefore, the timing deviation throughout the 100 μs is constant within the 200 ps time resolution and can be considered as stable.
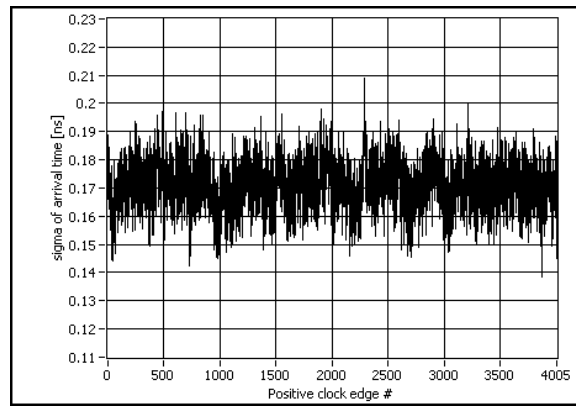
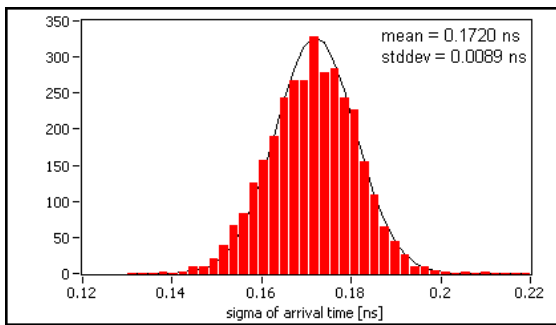**Figure 6.37:** Deviation of clock arrival time versus its number.

Figure 6.38: Deviation of clock arrival time: $R^2 = 0.9838$.
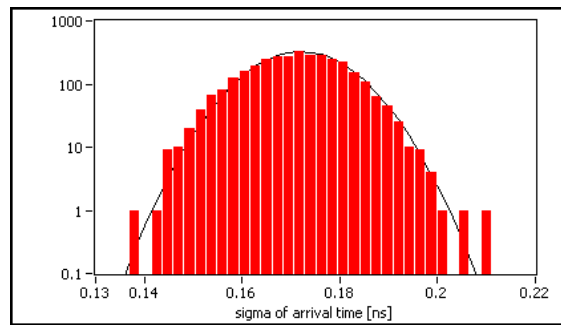

Figure 6.39: Logarithmic plot of the deviation of clock arrival time.

Clock period

Figure 6.40 and Figure 6.41 show linear and logarithmic histograms of the clock period time.
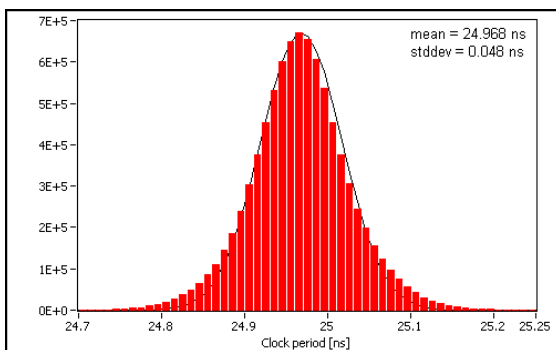

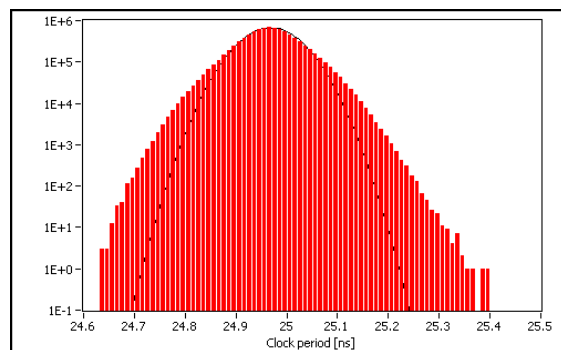**Figure 6.40:** Clock period: $R^2 = 0.9915$.

Figure 6.41: Logarithmic plot of the clock period time.

The jitter on the clock period time is 48 ps and therefore much lower than the theoretical limit of 200 ps$/\sqrt{3} = 115$ ps. This was achieved by fitting a third order

polynomial to the sampling points around the clock edges and thus increase accuracy (see section 6.2.4).

Orbit period

Figure 6.42 and Figure 6.43 show linear and logarithmic histograms of the orbit period time.
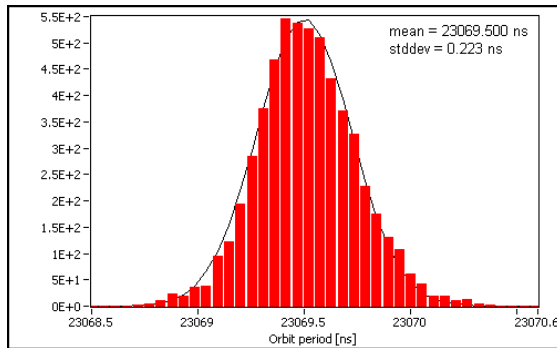

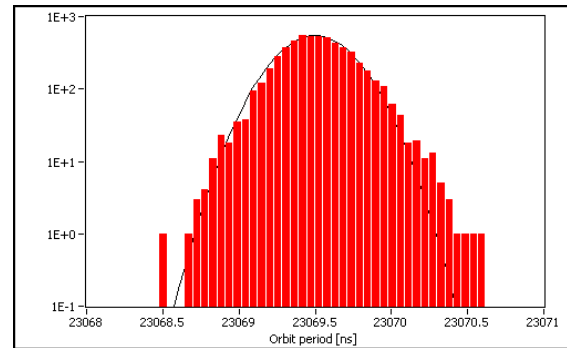**Figure 6.42:** Orbit period: $R^2 = 0.9928$.

Figure 6.43: Logarithmic plot of the orbit period time.

Although the same fits were done for the orbit signal as for the clock signal, the jitter on the orbit period time is higher than the time resolution of oscilloscope. This implies that there is probably a small jitter on the orbit signal of about 100 to 200 ps.

6.2.6   BPTX signal noise

Noise without beam

Several 100 μs traces were taken when the SPS beam was not running to determine the noise (see Figure 6.44).
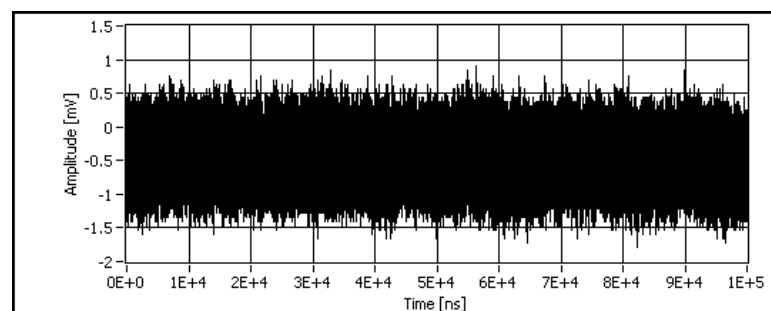

Figure 6.44: Example trace of the BPTX signal noise without SPS beam.

The measurement was DC coupled. The vertical range for these acquisitions was 16.38 mV, thus the lsb was 64 μV. The results are shown in Figure 6.45 and Figure 6.46.
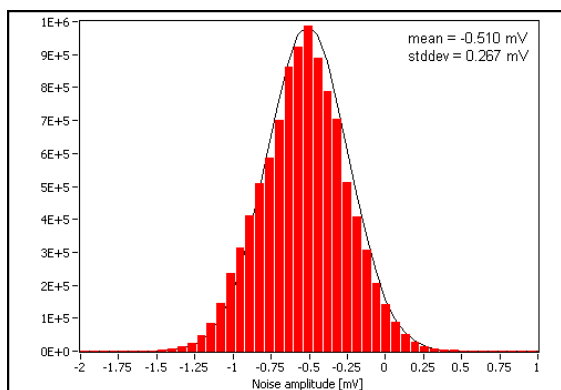
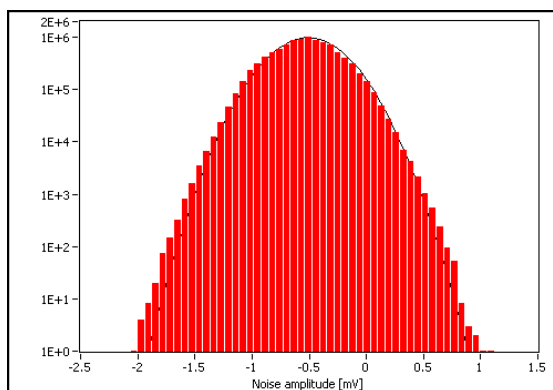**Figure 6.45:** Noise amplitude without beam: $R^2 = 0.9897$.

Figure 6.46: Logarithmic plot of the noise amplitude.

Noise with beam

Again, several 100 μs traces were taken when the SPS beam was running to measure the noise (see Figure 6.47). To determine just the signal noise and not only the digitisation noise, special care was taken to capture the BPTX signal in between the bunch patches (i.e. the abort gap).
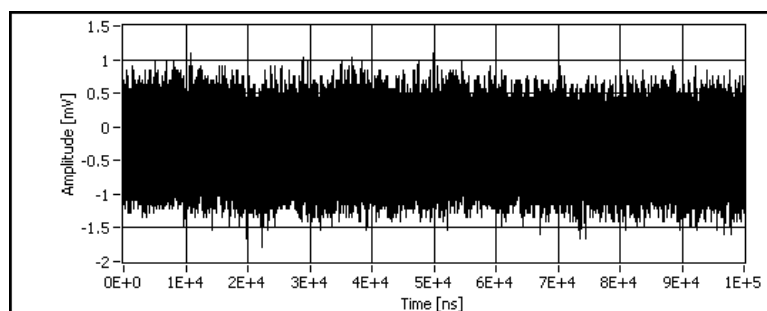
Figure 6.47: Example trace of the BPTX signal noise with SPS beam running.

This measurement was DC coupled as well. The vertical range was also 16.38 mV, therefore the lsb was again 64 μV. The results are shown in Figure 6.48 and Figure 6.49.

The noise is about four orders of magnitude lower than the bipolar bunch signal itself (see Figure 6.23). There also were several traces taken with coupling resistances and capacitances to the shielding of the transmission line before the oscilloscope (with 5 and 10 Ω and 10 pF) in order to distort the signal. However, the BPTX signal could still be processed and the bipolar bunch signals could still be distinguished from the noise, both with AC and DC coupling. This was done because the input of the oscilloscope needs to be decoupled in the final system.
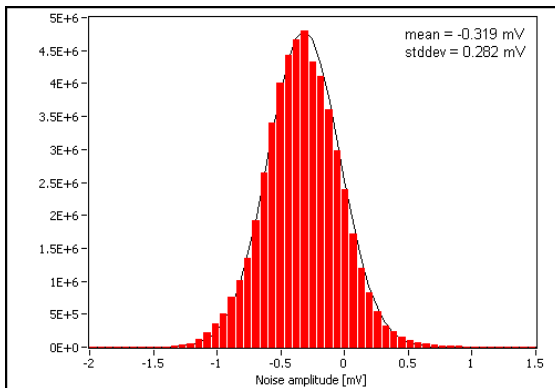
Figure 6.48: Noise amplitude with beam: $R^2 = 0.9966$.
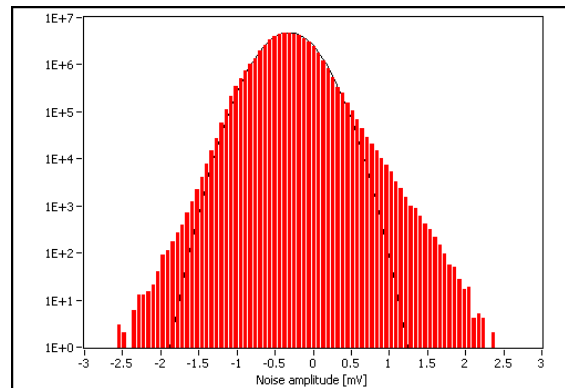
Figure 6.49: Logarithmic plot of the noise amplitude.

6.2.7 Conclusions

These tests show that the read-out system for the CMS BPTX works very well with real signals. It sees the bunches in real time (see Figure 6.12) and is therefore going to be a key real time debugging tool for the LHC. The system also proves to be very stable when it comes to dealing with noise. The final read-out will be based on the LeCroy WR64Xi oscilloscope, which, after a review of the processing software, will probably have an update rate of 1 Hz and therefore be able to provide data via the CERN Data Interchange Protocol (DIP). The interface will be implemented in standard BRM software framework (see [33]).

Chapter 7

Conclusions

In this thesis, the design, implementation and testing of a system was introduced, which is able to measure intensities and lengths of individual bunches as well as to monitor their phase with respect to a clock and the beam structure. The fast and complicated signals from the BPTX stations are acquired with a commercial oscilloscope and then processed with an analysis software developed in LabVIEW.

A mathematical model describing the shape and size of the BPTX signals was also portrayed. To get the correct signal features, the effects of the transmission line and the oscilloscope bandwidth were included. Using this model, the expected signal characteristics for several beam scenarios were computed.

The software of the monitoring system was described and its ways of retrieving information from the various signals were presented. The method of allocating each recognised bunch with a phase and a BCID was also shown. So as to ensure not only an overview of but also detailed insight into the many parameters the system will measure, several modules were designed to work up the data for the user.

The stability and performance of the analysis software were evaluated during a thorough long-run test of the full analysis chain with a simulated signal set up in the electronics laboratory. Furthermore, the various candidates for the oscilloscope were tested on their communication speed and stability with a standard CMS Rack-PC used in final system. Measurements done at the SPS accelerator indicate that the read-out system for the CMS BPTX works very well with real signals and the signal model agrees rather well with the real signal shape and amplitude.

The system design presented here fulfils all requirements except the ones that require involvement of other CMS subsystems (e.g. receiving machine information via DIP, long-term database storage, etc.). To conclude, after the LHC will have started operation, the beam monitoring system will be a key real time debugging tool for the LHC and a vital part in simplifying the timing-in of the subdetectors.

Appendix A

BPTX signal cable

A.1   Length measurement

The length of the cables installed between the rack in the CMS counting room USC55 and the BPTX stations were measured using a Time Domain Reflectometer (see [34]). This metallic TDR cable fault locater is usually used to look for cable defects. It simply sends a pulse through the cable and measures the time between the original pulse and any reflection. Thus it can also be used for measuring cable length.

There are two cables installed per pick-up, i.e. two coming from the left side and two from the right side of the detector. Only one from each pair will finally be connected to the sum signal of the four electrodes of the BPTX.
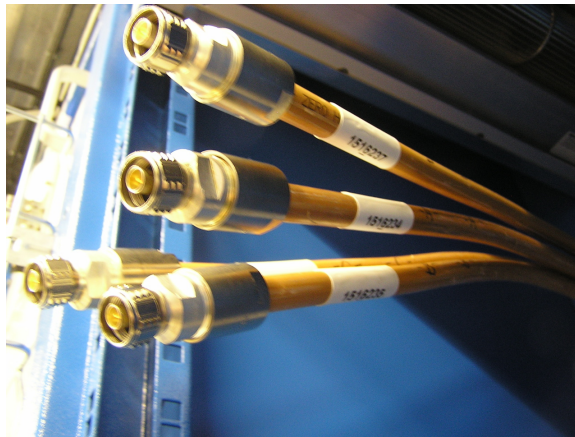
Figure A.1: CMS BPTX cables in the S1E08 rack.

After measuring the delay of the pulse reflection, the cable length can be calculated using the velocity of propagation (VOP), a parameter that characterizes the speed at which an electrical signal passes through a the cable. It is the ratio of a signal's transmission speed compared to the speed of light and was given to be 81% (see [17]).

The time delay and the calculated cable lengths are shown in Table A.1.

Table A.1: Measured cable delays from the TDR instrument and resulting lengths.

Name	Label	Delay [μs]	Length [m]
A	1516234	1.0074	244.63
B	1516235	1.0069	244.51
C	1516236	0.9282	225.40
D	1516237	0.9280	225.35

A.2 Attenuation

In the cable data sheet also the attenuation per 100 m is given (see [17]). The values for the different frequencies are shown in Table A.2

Table A.2: Cable attenuation.

Frequency [MHz]	Attenuation [dB/100m]	
	Nominal	Maximum
80	2.28	2.50
160	3.32	3.60
450	5.94	6.40
900	8.93	9.50

Bibliography

[1] W. Demtröder. *Experimentalphysik 4*. Springer, 2002.

[2] P. Collier. *Standard filling schemes for the various LHC operation modes*. LHC-OP-ES-0003, September 2004.

[3] K. Schindl. *The Injector Chain for the LHC*. LHC Project Workshop IX, Chamonix, France, January 1999.

[4] A. Beuret et al. *The LHC Lead Injector Chain*. EPAC, Lucerne, Switzerland, July 2004.

[5] CMS Coll. *The CMS experiment at the CERN LHC*. Submitted to JInst., 2008.

[6] CMS Coll. *The Trigger and Data Acquisition project, Volume I, The Level-1 Trigger, Technical Design Report*. CERN/LHCC 2000-038, CMS TDR 6.1, 2000.

[7] CMS Coll. *The Trigger and Data Acquisition project, Volume II, Data Acquisition and High-Level Trigger, Technical Design Report*. CERN/LHCC 2002-026, CMS TDR 6, 2002.

[8] S. Baron. *TTC challenges and upgrade for the LHC*. 11th Workshop on Electronics for LHC and Future Experiments, Heidelberg, Germany, September 2005.

[9] Z. Guzik and R. Jacobsson. *Beam Phase and Intensity Monitor (BPIM) for the LHCb Experiment*. 12th Workshop on Electronics for LHC and Future Experiments, Valencia, Spain, September 2006.

[10] S. Baron and M. Joos. *RF2TTC V3, User Manual V2.1, RF to TTC VMEbus Interface Card and S/W*. PH-ESS-16-05-2007, May 2007.

[11] L. Fernandez-Hernando et al. Development of a CVD diamond Beam Condition Monitor for CMS at the Large Hadron Collider. *Nucl. Instrum. Meth. A*, 552:183, 2005.

[12] A. Macpherson. Beam Condition Monitoring and radiation damage concerns of the experiment. *Proceedings of the XV LHC Project Chamonix Workshop, Divonne*, page 198, 2006.

[13] D. Chong et al. Validation of synthetic diamond for a Beam Condition Monitor for the Compact Muon Solenoid Experiment. *IEEE Trans. Nucl. Sci.*, 54:182, 2007.

[14] C. Ohm. *Phase and Intensity Monitoring of the Particle Beams at the ATLAS Experiment.* Master Thesis (submitted), 2007.

[15] D. P. McGinnis. *The design of beam pickup and kickers.* Fermi National Accelerator Laboratory, AIP Conf. Proc., Volume 333, May 1995.

[16] LHC proton parameters. Website. Available online at http://edms.cern. ch/cedar/plsql/navigation.tree?top=CERN-0000020013; visited on Ausgust 31st 2007.

[17] Nexans HF-50 - 1/2" - ALUH. Website. Available online at https://twiki.cern.ch/twiki/bin/viewfile/Atlas/AtlasBPTX?rev=1;filename= HF-50_-_1_2_-_ALUH.pdf; visited on September 11th 2007.

[18] C. Boccard. *Measured value for the capacitance between beam and button electrode.* CERN AB/BI. Private communication.

[19] D. Fleischmann. *Basiswissen Elektrotechnik.* Vogel, 1999.

[20] T. Aumeyr. *Evaluation of Oscilloscopes for the BPTX Read-Out System - Tests in the ATLAS Trigger Electronics Lab.* CMS-IN-2007/049, September 2007.

[21] T. Aumeyr. *Evaluation of the oscilloscope-based BPTX read-out during SPS operation.* CMS-IN-2007/047, September 2007.

[22] LeCroy WavePro 7000A series. Website. Available online at http://www.lecroy. com/tm/products/Scopes/WavePro_7000A/LeCroy_WavePro_DC_High.pdf; visited on Ausgust 29th 2007.

[23] LeCroy Waverunner Xi series. Website. Available online at http://www. lecroy.com/tm/products/Scopes/WaveRunner_Xi/WRXi_datasheet.pdf; visited on Ausgust 28th 2007.

[24] Tektronix DPO4000 series. Website. Available online at http://www.tek.com/ site/ps/48-19032/pdfs/48W_19032.pdf; visited on Ausgust 29th 2007.

[25] Tektronix DPO7000 series. Website. Available online at http://www.tek.com/ site/ps/4M-19046/pdfs/4MW_19046.pdf; visited on Ausgust 28th 2007.

[26] Ph. Farthouat and P. Gällnö. *TTC-VMEbus INTERFACE.* RD12 Project, May 2000.

[27] P. Borrego Amaral et al. *The ATLAS Local Trigger Processor (LTP).* ATL-DAQ-2004-016, November 2004.

[28] U. Schroffenegger. *Linux drivers for LeCroy oscilloscopes.* LeCroy, Meyrin. Private communication.

[29] SPS Scrubbing Run. Website. Available online at https://webh09.cern.ch/ ab-mgt-md-users/2007/SPSScrubbingRun24.htm; visited on Ausgust 28th 2007.

[30] General information for the LHC beam with 25 ns spacing. Website. Available online at https://pcr-consigns.web.cern.ch/PCR-Consigns/beam-settings/ LHC/2007_LHC_25NS_SPACING/LHC_Instr_frames.htm; visited on Ausgust 28th 2007.

[31] LHC-BOBR-ES-0001. *The Beam Synchronous Timing Receiver Interface for the Beam Observation Systems*, September 2003.

[32] LHC Machine Timing Distribution for the Experiments. Website. Available online at http://ttc.web.cern.ch/TTC/intro.html; visited on Ausgust 28th 2007.

[33] R. Hall-Wilton et al. *Results from the Slice Test of the BCM2 Subdetector for the CMS Beam Conditions Monitor*. CMS-IN-2007/037, May 2007.

[34] RiserBond Time Domain Reflectometer Model 1270A. Website. Available online at http://www.riserbond.com/doclib/1270a_br2007.pdf; visited on September 11th 2007.